Thermoelectric ceramics based on the layered calcium cobaltite doped by bismuth oxide

Andrei I. Klyndyuk[a,*], Iryna V. Matsukevich[b], Roman S. Latypov[a], Peter Veteška[c], Ondrej Hanzel[d], Ekaterina A. Chizhova[a], Marián Janek[c]

[a]*Department of Physical, Colloid and Analytical Chemistry, Belarusian State Technological University, 220006 Minsk, Belarus*

[b]*FunGlass – Center for Functional and Surface Functionalized Glass, Alexander Dubček University of Trenčin, 911 50 Trenčín, Slovakia*

[c]*Department of Inorganic Materials, Slovak University of Technology in Bratislava, 812 37 Bratislava, Slovakia*

[d]*Institute of Inorganic Chemistry, Slovak Academy of Sciences, 845 36 Bratislava, Slovakia*

*Corresponding author.

E-mail address: klyndyuk@belstu.by (A.I. Klyndyuk)

Abstract. Using solid-state reaction method, the ceramics of $Ca_3Co_4O_{9+\delta}$ doped by Bi_2O_3 was prepared, its microstructure and properties were investigated. The single-phase $(Ca,Bi)_3Co_4O_{9+\delta}$ solid solutions formed at substitution of up to 10 mol. % calcium by bismuth, but at larger bismuth content samples consisted of $(Ca,Bi)_3Co_4O_{9+\delta}$ and $Bi_2Ca_2Co_{1.7}O_y$. Increasing of Bi_2O_3 content in the samples leads to decreasing electrical resistivity and increasing of Seebeck coefficient, but thermal conductivity changed unmonotonously, increasing for single-phase ceramics and decreasing for composite one. Thermoelectric characteristics of $Ca_3Co_4O_{9+\delta}$ are essentially enhanced by its doping using

Bi_2O_3, and the best thermoelectric performance was demonstrated by the $Ca_{2.4}Bi_{0.6}Co_4O_{9+\delta}$ composite material, whose power factor and figure-of-merit values reach 284 $\mu W \cdot m^{-1} \cdot K^{-2}$ and 0.279, which are 4.6 and 4 times larger than for the parent phase. Such improvement in the thermoelectric efficiency of $Ca_3Co_4O_{9+\delta}$ is provided by substitution of calcium by bismuth and through creation of phase inhomogeneity in ceramics.

Keywords: $Ca_3Co_4O_{9+\delta}$-based ceramics; Bi_2O_3 doping; Phase inhomogeneity; Thermoelectric performance

Highlights

- $(Ca,Bi)_3Co_4O_{9+\delta}$ ceramics prepared by solid-state reactions route comprehensively studied
- Bi_2O_3 doping decreases electrical resistivity of ceramics
- Phase inhomogeneity of prepared ceramics increases its Seebeck coefficient
- $Ca_{2.4}Bi_{0.6}Co_4O_{9+\delta}$ ceramics shows the best thermoelectric performance

1. Introduction

The lost technological heat, evolving into environment during working of factories, power plants or transportation, can be utilized and converted into electrical energy using devices called thermoelectric generators (TEGs). The TEGs are based on special group of materials named thermoelectrics, demonstrating good electrical conductivity, bad thermal conductivity and high values of Seebeck coefficient [1]. For high-temperature applications, the most promising thermoelectrics are metal oxides, which are stable at high temperatures in air and, in contrast to the traditional thermoelectric materials based on the layered chalcogenides of bismuth, lead or tin, do not contain rare, expensive, and toxic components [2].

The promising materials for *n*-legs of TEGs are solid solutions of calcium manganite ($CaMnO_3$) [3,4] or strontium titanate ($SrTiO_3$) [5,6] with perovskite structure (ABO_3). On the other hand, the optimal base for *p*-legs of TEGs are derivatives of layered cobaltites of sodium (Na_xCoO_2) [7,8], calcium ($Ca_3Co_4O_{9+\delta}$) [9,10] or bismuth–calcium ($Bi_2Ca_2Co_{1.7}O_y$) [11,12] etc. Layered calcium cobaltite is typical misfit-layered phase which crystal structure consists of [Ca_2CoO_3] and [CoO_2] layers having different periodicity in one direction [13]. Low values of electrical resistivity (ρ) of this phase is due to high concentration of main charge carriers ("holes") in conducting [CoO_2]–layeres, while relatively high values of Seebeck coefficient is connected to presence of cobalt ions in different charge and spin states. The misfit-layered structure of $Ca_3Co_4O_{9+\delta}$ cobaltite causes low values of its thermal conductivity [14].

To improve thermoelectric performance of layered calcium cobaltite and make it suitable for practical usage a number of strategies are used: *i*) partial substitution in its structure of calcium by rare-earth elements [15,16] or bismuth [17–19] and/or cobalt by

transition and heavy metals [20–22]; *ii*) using "solution" synthesis methods [23,24] or self-propagating high-temperature synthesis to achieve small particle size distribution in desired phase [25]; *iii*) instead conventional sintering applying other sintering methods, such as hot-pressing [10,23,26], spark plasma sintering [24,26,27], oscillatory pressure sintering [28], or so-called two-step sintering [29–31] to enhance interparticle contacts; *iv*) modification of ceramics by micro- or nanoparticles of metals [31–34], metal oxides [35,36] or carbides [37,38] to modulate material electrical conductivity; *v*) creation in ceramics chemical [39] or phase inhomogeneity [10,27,31] due to its self-doping (producing ceramics with composition beyond its phase homogeneity area) to ensure decrease in thermal conductivity; *vi*) producing of ceramics with high configurational entropy of one or some cationic sublattices (high-entropy strategy) [6,40–42] to improve material physical and chemical properties. It has been shown by different authors [10,23–31], that using of special sintering methods results in the formation of ceramics with lower porosity and electrical resistivity values. According to our previous investigations [10,30,31] and literature data [27,31–33,35–39], chemically and phase-inhomogeneous ceramics usually demonstrated larger values of Seebeck coefficient than the single-phase one.

Despite common (trivial) character of substitution (doping) strategy, its effectiveness and importance, particularly at development of thermoelectric oxide ceramics, are without doubts. Effect of bismuth substitution for cobalt in $Ca_3Co_4O_{9+\delta}$, firstly described in [9], was verified in later studies [43–58], either alone [45,48–50,52,54] or in combination with variation of synthesis/sintering methods [46,47,55–58] as well as at using bismuth as co-doping element [43,44,51,53] to optimize the material

thermoelectric properties. Phase equilibria in the Bi_2O_3–CaO–CoO_y system in a wide temperature range were therefore described in [59,60].

The main reason of interest paid to the bismuth-containing derivatives of layered calcium cobaltite is due to they can be relatively easily produced by means of traditional solid-state reaction method and conventional sintering. Due to their good thermoelectric performance and mechanical properties, these compounds are often used as materials for *p*-legs of thermoelectric modules and TEGs of different constructions [61–63].

Preliminary results of our investigations of effect of substitution of calcium or/and cobalt in $Ca_3Co_4O_{9+\delta}$ on its structure, electrical, thermal, and thermoelectric properties are described in [19,21,50,51].

Though bismuth-containing layered calcium cobaltite was an object of investigation of many works listed above, some questions still remain unsolved. Firstly, the results of different works often have not coincided with each other. Secondly, it is still unclear which factor – chemical composition, phase composition (phase inhomogeneity), microstructure, etc. – is mainly responsible for improving of thermoelectric performance of $Ca_3Co_4O_{9+\delta}$ at its doping with bismuth oxide. So, further study of this system must actually help better clarify up to date summarized results.

In this work, $Ca_{3-x}Bi_xCo_4O_{9+\delta}$ (x = 0.0, 0.2, 0.3, 0.5, 0.6) thermoelectric ceramics were obtained using solid-state reactions route and conventional sintering. The materials prepared were characterized by X-ray diffraction (XRD) and their microstructure by scanning electron microscopy combined with energy-dispersive X-ray spectroscopy (SEM/EDX). The ceramics thermal (thermal expansion, thermal diffusivity, thermal conductivity), electrical (electrical resistivity, Seebeck coefficient), and thermoelectric properties (power factor, figure-of-merit) in a wide range of temperatures were studied.

Effects of substitution of cobalt for bismuth and creation of phase inhomogeneity in ceramics on its properties were therefore strategically isolated to clarify their effect.

2. Experimental section

2.1. Synthesis and preparation of the samples

$Ca_{3-x}Bi_xCo_3O_{9+\delta}$ (x = 0.0, 0.2, 0.3, 0.5, 0.6) powders were prepared using solid-state reaction route from $CaCO_3$ ("analytically pure grade", min. 99.0 wt. %, VEKTON, Russian Federation), Bi_2O_3 ("pure grade", min. 99.0 wt. %, VEKTON, Russian Federation), and Co_3O_4 ("pure grade", min. 99.0 wt. %, VEKTON, Russian Federation) powders through reaction (1):

$$(3–x)CaCO_3 + x/2Bi_2O_3 + 4/3Co_3O_4 + (1/3+\delta/2–x/4)O_2 = Ca_{3-x}Bi_xCo_4O_{9+\delta} + (3–x)CO_2. \quad (1)$$

They were separately weighed following required stoichiometric amounts, then thoroughly mixed in a Fritch Pulverizette 6.0 planetary mill (Fritch Germany) with addition of ethanol (ZrO_2 grinding vials and balls, 300 rpm for 1 h), pressed at 100–150 MPa into pellets 22 mm in diameter and 5–7 mm in thickness, and calcined in a muffle furnace in air at 1173 K for 12 h. After samples were crushed in an agate mortar, milled in a Fritch Pulverizette 6.0 planetary mill (Fritch Germany) with addition of ethanol (ZrO_2 grinding vials and balls, 300 rpm for 1 h), uniaxial pressed at 100–150 MPa into bars 5×5×30 mm in dimensions and pellets 15 mm in diameter and 2–3 mm in thickness, and sintered in air at 1193 K for 12 h. The sintered samples were then used for the study of their electrophysical and thermophysical properties.

2.2. Characterization of equipment and procedures

The phase composition of the samples and crystal structure of the major phase in them ($Ca_3Co_4O_{9+\delta}$ and its solid solutions) were investigated using XRD analysis (Bruker D8 XRD Advance diffractometer (Bruker, USA) (Cu–K_α–radiation, Ni–filter)).

Values of the coherent scattering areas (CSAs) and microstrains (ε) of the sintered ceramic samples were calculated using Sherrer equation (D_S) [64], Williamson–Hall ($D_{W–H}$) [65] and size–strain ($D_{S–S}$) methods [66], which are described in Supplementary information (equations (S1)–(S3)). The degree of crystallographic orientation of the grains (texturing) of the $Ca_{3–x}Bi_xCo_3O_{9+\delta}$ ceramics was evaluated using the Lotgering factor (f) (equation (S4)) [67].

Values of pycnometric density of powders (d_{pow}) (the base density) and sintered ceramics (d_{cer}) were measured by means of gaseous pycnometer Ultrapycnometer 1000 (Quantachrome Instruments, USA) (pycnometric gas is helium) and by Archimedes method [68] respectively, and based on them the values of the porosity of the samples (P) were calculated as

$$\Pi = ((d_{pow} - d_{cer})/d_{pow}) \cdot 100\%. \quad (2)$$

The microstructure of the sintered ceramics and its chemical composition were studied by scanning electron microscopy (SEM) using JEOL 7500F (Japan) scanning electron microscope equipped with an energy-dispersive spectroscopy (EDS) detector. Prepared specimens were observed using SEI (secondary electron image) detector at acceleration voltage of 15 kV, probe current of 8 μA and working distance of 6–7 mm. EDS analysis was done using AZtec software at acceleration voltage of 15kV and probe current of 15 μA.

Electrical resistivity (ρ) and Seebeck coefficient (S) of the samples were measured within 300–1073 K by applying of LINSEIS LSR–3 measuring system (Linseis, Germany) in a helium atmosphere ($p_{He} \approx 0.15$ bar). The values of the weighted mobility (μ) of the charge carriers and their concentration (p) in the samples were calculated based on the experimentally obtained values of ρ and S of ceramics studied

according to [69] as it is described in Supplementary information (equations (S5)–(S6)). Apparent activation energy of electrical conductivity values (σ) of the samples (E_A) were found from the linear parts of $\ln(\sigma \cdot T) = f(1/T)$ plots.

Thermal expansion of the sintered ceramics was investigated using Thermomechanical Analyzer Netzsch TMA 402 F1 Hyperion (Netzsch, Germany) within 293–1073 K in an N_2 atmosphere at heating rate of 10 K/min. The samples were fixed with a constant force of 50 mN. Values of the average linear thermal expansion coefficient (α, LTEC) were determined from the linear parts of $\Delta l/l_0 = f(T)$ plots, respectively. The thermal diffusivity (η) of the samples was measured in the helium atmosphere within the temperature interval of 293–873 K by means of laser flash method (Linseis LFA 1000, Germany). The thermal conductivity values (λ) of the ceramics were calculated according to the equation

$$\lambda = \eta \cdot d_{cer} \cdot C_p, \quad (3)$$

where C_p is the heat capacity determined by the Dulong–Petit law.

The phonon (λ_{ph}) and electronic parts (λ_{el}) of thermal conductivity of ceramics were isolated by means of equations (4,5)

$$\lambda = \lambda_{ph} + \lambda_{el}, \quad (4)$$

$$\lambda_{el} = L \cdot T/\rho, \quad (5)$$

where L is the Lorentz number, $L = 2.45 \cdot 10^{-8}$ $V^2 \cdot K^{-2}$.

The power factor (PF) and figure-of-merit values (ZT) of the samples were calculated as

$$PF = S^2/\rho, \quad (6)$$

$$ZT = PF \cdot T/\lambda. \quad (7)$$

3. Results and discussion

3.1. Phase composition and crystal structure

The single-phase $Ca_{3-x}Bi_xCo_4O_{9+\delta}$ solid solutions, as proved by the powder XRD patterns, were obtained at substitution of calcium by bismuth for up to 10 mol. % ($x \le 0.3$) (Fig. 1, scans 2–3), which is in a good agreement with the literature data [17–19, 46, 48, 50, 59, 60] and they possessed a monoclinic structure that was the same as for $Ca_3Co_4O_{9+\delta}$ parent phase (Fig. 1, scan 1) (PDF–2, Card № 00–021–0139, [13]). Samples with $x = 0.5$, 0.6 were non-single-phase and contained, along with the $Ca_{3-x}Bi_xCo_4O_{9+\delta}$ solid solution, the $Bi_2Ca_2Co_{1.7}O_y$ phase [11], which reflexes on the XRD patterns became stronger at x increasing (Fig. 1, scans 4–5).

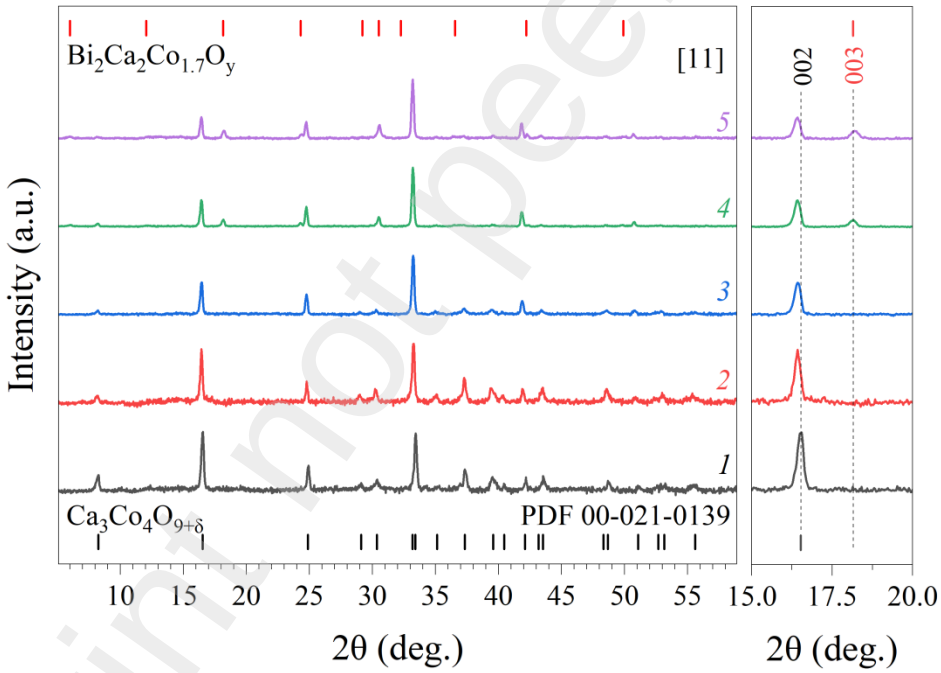

Fig. 1. XRD patterns of the powdered $Ca_{3-x}Bi_xCo_4O_{9+\delta}$ samples at room temperature (Cu–K_α radiation): $x = 0.0$ (*1*), 0.2 (*2*), 0.3 (*3*), 0.5 (*4*), and 0.6 (*5*). The panel to the right shows an enlarged XRD patterns view at 2θ 15–20 degrees

Our results coincide with the data of [59,60], according to them the saturated $Ca_{2.7}Bi_{0.3}Co_4O_{9+\delta}$ solid solution coexists with the $Bi_2Ca_2Co_{1.7}O_y$ layered ternary oxide possessing monoclinic structure and cobalt oxide. The absence of reflexes of cobalt oxide on the XRD patterns (Fig. 1) is, probably, due to its small quantity lying beyond the detection limit of XRD method or its presence in the mixtures in partial or fully amorphized form. The reflexes of $Ca_{3-x}Bi_xCo_4O_{9+\delta}$ solid solutions shifted to the lower angles at $x \leq 0.3$ (Fig. 1, scans 1–3, right panel) due to partial substitution of smaller Ca^{2+} ions by larger Bi^{3+} ones (values of ionic radii of Ca^{2+} and Bi^{3+} ions for C.N. = 6 are equal to 0.100 and 0.102 nm respectively [70]), but on the XRD patterns of the samples with $x = 0.5$, 0.6, their positions, as the positions of reflexes of $Bi_2Ca_2Co_{1.7}O_y$ phase, were practically unchanged (Fig. 1, scans 4–5, right panel) proving their constant composition.

3.2. Microstructure and elemental analysis

Apparent density values of both powdered and sintered samples increased, and ceramic porosity decreased at increasing of bismuth oxide content in it (Table 1), indicating that Bi_2O_3 addition results in improving of sinterability of the layered calcium cobaltite-based ceramics. The Π values for both single-phase and composite $Ca_{3-x}Bi_xCo_4O_{9+\delta}$ ceramics were comparatively close to each other, which shows that creation of phase inhomogeneity in $Ca_3Co_4O_{9+\delta}$ slightly affects its sinterability and coincides with the results [10] in which the same was observed for self-doped composite ceramics.

The microstructure of ceramics studied was layered and consisted of grains in form of plates (flakes) of 1.4–2.3 μm (l) in size and thickness of about 0.8–1.3 μm (h), which values, in the whole, increased at increasing substitution degree of calcium by bismuth, but the aspect ratio (AR = l/h) observed had nearly the same values (1.6–1.7)

for all the compositions studied. The grains were partially aggregated in stacks and, for the samples with $x > 0.2$, predominantly oriented in the direction perpendicular to the pressing axis.

Table 1. Values of pycnometric density of $Ca_{3-x}Bi_xCo_4O_{9+\delta}$ powders (d_{pow}) and ceramics (d_{cer}), and its porosity (Π)

x	d_{pow} (g·cm^{-3})	d_{cer} (g·cm^{-3})	Π (%)
0.0	4.64	2.64	43.1
0.2	4.67	3.28	29.8
0.3	4.85	3.64	24.9
0.5	5.06	3.27	35.4
0.6	5.19	4.04	22.2

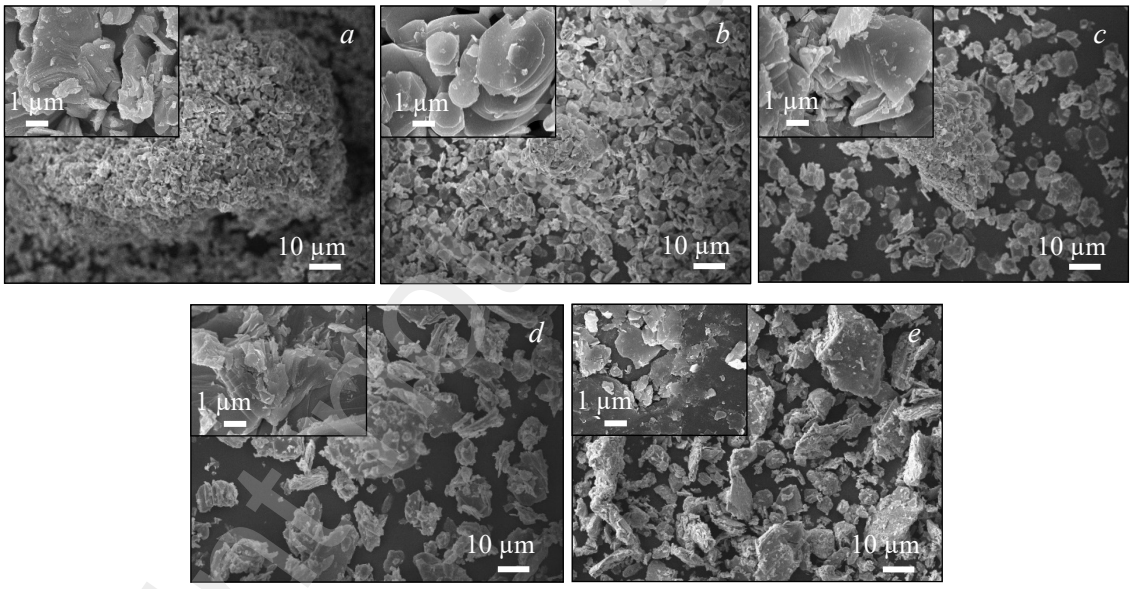

Fig. 2. SEM images of the surface sections for sintered $Ca_{3-x}Bi_xCo_4O_{9+\delta}$ ceramic samples: (*a*) $x = 0.0$, (*b*) $x = 0.2$ (2), (*c*) $x = 0.3$, (*d*) $x = 0.5$, and (*e*) $x = 0.6$

The Lotgering factor values increased from 0.29–0.33 (moderate orientation) to 0.52–0.69 (good orientation) for the samples with $0.0 \le x \le 0.2$ (single-phase ceramics) and

$0.3 \le x \le 0.6$ (composite ceramics), respectively (Table S1). Thus, formation in $Ca_3Co_4O_{9+\delta}$-based ceramics of phase inhomogeneity through overdoping by bismuth oxide improves the degree of crystallographic grains orientation (degree of texturing). Coherent scattering area values, corresponding to the crystallite sizes, for the $Ca_{3-x}Bi_xCo_4O_{9+\delta}$ samples calculated using different methods varied within 28–38 nm and increased at x increasing, and microstrains varied within $(2–29)\cdot10^{-4}$ reaching maximal values for the samples lying near border between single- and non-single-phase ceramics (Table S1). As can be seen, partial substitution of calcium by bismuth in $Ca_3Co_4O_{9+\delta}$ results in increasing of CSA of ceramics up to 15–30 %.

According to the EDS results, the cationic composition of the $Ca_{3-x}Bi_xCo_4O_{9+\delta}$ synthesized compounds was very close to the target values (taking into account the error of measurements – ±5 mol. %) (Table 2, Figs. S1–S3), and all the elements were evenly distributed within the ceramic, as indicated by the results of EDS mapping of the surface of ceramics (Figs.2 and S4–S6).

Table 2. Nominal and real (obtained by EDX results) composition of the samples

Sample	Nominal composition (mol. %)			Real composition (mol. %)		
	$BiO_{1.5}$	CaO	CoO_x	$BiO_{1.5}$	CaO	CoO_x
$Ca_3Co_4O_{9+\delta}$	–	42.86	57.14	–	39.76	60.24
$Ca_{2.8}Bi_{0.2}Co_4O_{9+\delta}$	2.86	40.00	57.14	2.96	33.88	63.16
$Ca_{2.7}Bi_{0.3}Co_4O_{9+\delta}$	4.29	38.57	57.14	4.71	32.86	62.43
$Ca_{2.5}Bi_{0.5}Co_4O_{9+\delta}$	7.14	35.71	57.14	7.78	30.40	61.83
$Ca_{2.4}Bi_{0.6}Co_4O_{9+\delta}$	8.57	34.29	57.14	12.31	30.00	57.69

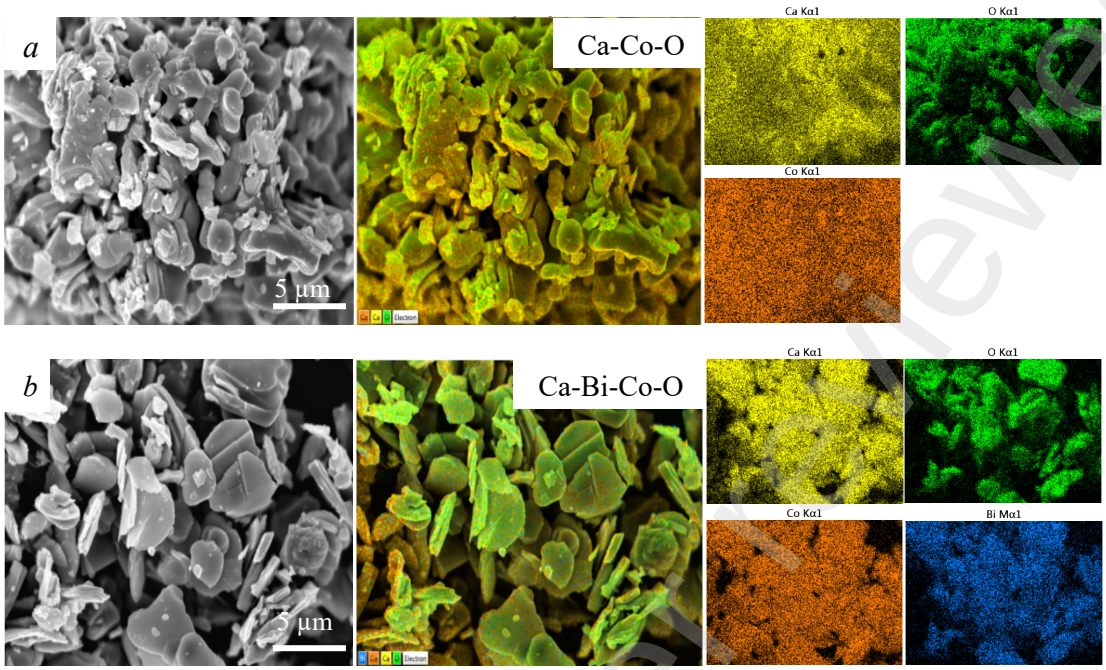

Fig. 3. Element mapping images of the $Ca_3Co_4O_{9+\delta}$ (*a*) and $Ca_{2.8}Bi_{0.2}Co_4O_{9+\delta}$ (*b*) ceramic samples

3.3. Electrical transport properties

As can be seen from the Fig. 4, $Ca_{3-x}Bi_xCo_4O_{9+\delta}$ cobaltites are the *p*-type semiconductors ($\partial\rho/\partial T < 0$), which conductivity character for the electrical resistivity of the samples with $x = 0.2$, 0.3 near 800 K changed into small-pronounced metallic-like one ($\partial\rho/\partial T > 0$) (Fig. 4, *a*). Dependencies of $S = f(T)$ were close to the linear which is typical for $Ca_3Co_4O_{9+\delta}$-based ceramics [10] and obeyed equation (8) [8, 71], which is commonly used for determination of thermoelectric power of metals and degenerated semiconductors:

$$S = \left(\frac{8\pi^2 k_B^2}{3eh}\right) m^* T \left(\frac{\pi}{3p}\right)^{2/3}, \qquad (8)$$

where k_B is the Boltzmann constant, m^* is the density of the effective mass of charge carriers, h is the Planck's constant, e is the electron charge, T is the absolute temperature, and p is the concentration of the charge carriers.

Electrical resistivity values of $Ca_{3-x}Bi_xCo_4O_{9+\delta}$ ceramic samples decreased at x increasing that was most pronounced for single-phase region (Fig. 4, *c*), and may be due to the decreasing of ceramic porosity (Table 1) and improving of quality of grain boundaries in its structure (taking into account donor character of the substitution of Ca^{2+} by Bi^{3+} it would be natural to expect the increasing of ρ values at such substitution, like it was observed for $Ca_{3-x}Bi_xCo_4O_{9+\delta}$ single-phase solid solutions in [19]). The minimal ρ value was observed for $Ca_{2.5}Bi_{0.5}Co_4O_{9+\delta}$ composite ceramics – 139 μΩ·m at 1100 K.

Seebeck coefficient values of ceramics expectedly (due to decreasing of charge carriers ("holes") concentration at substitution of $Bi^{3+} \rightarrow Ca^{2+}$) decreased in the single-phase region and increased with x increasing for composite ceramics (Fig. 4, *d*). The maximum value of S (211 $\mu V \cdot K^{-1}$ at 1100 K) was demonstrated by $Ca_{2.4}Bi_{0.6}Co_4O_{9+\delta}$ sample, which consisted of $Ca_{2.7}Bi_{0.3}Co_4O_{9+\delta}$ solid solution and $Bi_2Ca_2Co_{1.7}O_y$ phase. The positive effect of phase inhomogeneity on the Seebeck coefficient values of $Ca_3Co_4O_{9+\delta}$-based ceramics was many times detected earlier both for self-doped [10, 30], overdoped [19], and modified by other phases particles samples of layered calcium cobaltite [31,34]. Our results also prove the effectiveness of such approach in improving of thermoelectric performance of ceramics based on $Ca_3Co_4O_{9+\delta}$ phase. Note, in this case both phases which formed heterogeneous ceramics (monoclinic $Ca_{2.7}Bi_{0.3}Co_4O_{9+\delta}$ and $Bi_2Ca_2Co_{1.7}O_y$ phases), had the similar, layered structure, and phase inhomogeneity

was due to the self-doping of ceramics at shifting of its composition to the inhomogeneity region.

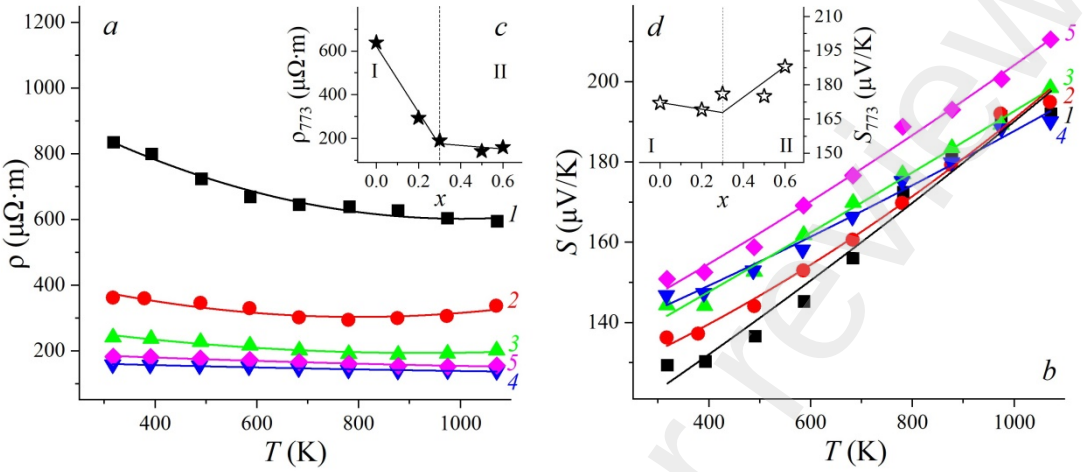

Fig. 4. Temperature (*a*, *b*) and concentration (*c*, *d*) dependences of electrical resistivity (ρ) (*a*, *c*) and Seebeck coefficient (*S*) (*b*, *d*) of the $Ca_{3-x}Bi_xCo_4O_{9+\delta}$ ceramics: x = 0.0 (*1*), 0.2 (*2*), 0.3 (*3*), 0.5 (*4*), and 0.6 (*5*). I – single-phase samples, II – non-single-phase samples

The values of the weighted mobility of charge carriers in ceramics decrease with increasing temperature due to an increase in their scattering at grain boundaries, defects in the crystal structure, and lattice sites (Fig. 5, *a*). Increasing of bismuth oxide content in $Ca_{3-x}Bi_xCo_4O_{9+\delta}$ ceramics results in increasing of weighted mobility of charge carriers and expected decreasing of their concentration; hereby, concentration dependencies of these parameters were similar (and nearly linear) for both homogeneous and heterogeneous ceramic samples (Fig. 5, *b*).

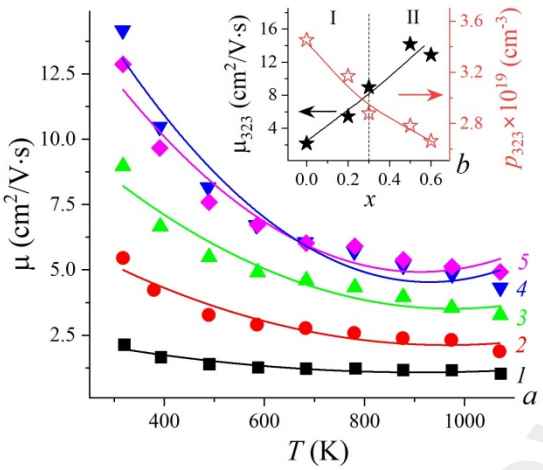

Fig. 5. Temperature (*a*) and concentration (*b*) dependences of weighted mobility of charge carriers (μ) and their concentration (*p*) in the $Ca_{3-x}Bi_xCo_4O_{9+\delta}$ compounds: x = 0.0 (*1*), 0.2 (*2*), 0.3 (*3*), 0.5 (*4*), and 0.6 (*5*). I – homogeneous ceramics, II – heterogeneous ceramics

On the Arrhenius plots of electrical conductivity ($\ln(\sigma T) = f(1/T)$ dependencies) of ceramics studied, one kink near 573 K matching Debye temperature of $Ca_3Co_4O_{9+\delta}$ phase (Θ_D = 572 K [57]) was detected (Fig. 6), like it was found in [72] for textured calcium cobaltite ceramics. The values of apparent activation energy of electrical conductivity (E_A) of $Ca_{3-x}Bi_xCo_4O_{9+\delta}$ ceramics below and above 573 K varied within 36–59 meV and 74–81 meV, respectively, and their values at x increasing decreased below Debye temperature for single-phase samples and increased above Debye temperature for composite samples (Fig. 6, inset). Found in this work E_A values of electrical conductivity for $Ca_{3-x}Bi_xCo_4O_{9+\delta}$ are coincided with values detected for layered calcium cobaltite in literature [10,19,30,72], that indicates the common

mechanism of electrical conductivity in materials studied, which is determined by the charge transfer within the $Ca_3Co_4O_{9+\delta}$ major phase of the samples.

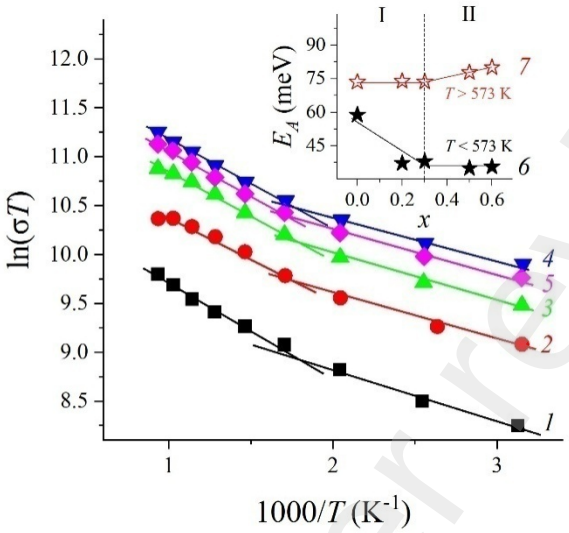

Fig. 6. Dependences of ln(σ*T*) versus reciprocal temperature for $Ca_{3-x}Bi_xCo_4O_{9+\delta}$ materials: x = 0.0 (*1*), 0.2 (*2*), 0.3 (*3*), 0.5 (*4*), and 0.6 (*5*). Inset shows concentration dependences of apparent activation of electrical conductivity of the samples below (6) and above (7) 573 K. I – homogeneous samples, II – heterogeneous samples

3.4. Thermal properties

Dilatometric curves ($\Delta l/l_0 = f(T)$ dependencies) for the studied sintered ceramic samples were practically linear, suggesting the absence of the structural phase transition of its main layered cobaltite phase in the temperature range of 293–1073 K, which coincides with the literature data [16,51,56]. The values of LTEC varied within (11.60–13.17)·10^{-6} K^{-1} (Table 3) and decreased at doping of parent compound ($Ca_3Co_4O_{9+\delta}$) by bismuth oxide, which was, probably, due to the increasing of energy of metal-oxygen interactions at partial substitution of less charged Ca^{2+} ion by more charged Bi^{3+} one, as

well as due to the decreasing of porosity of the samples at increasing of bismuth oxide content in them (Table 1). The LTEC values for parent phase and some of its derivatives coincide with the literature data [16,51], and lowering of LTEC of the $Ca_3Co_4O_{9+\delta}$ at its doping by bismuth oxide indicates that such doping improves thermomechanical properties of parent phase.

Table 3. LTEC (α) values of $Ca_{3-x}Bi_xCo_4O_{9+\delta}$ ceramics

x	0.0	0.2	0.3	0.5	0.6
$\alpha \cdot 10^6$, K^{-1}	13.17±0.66	13.00±0.65	12.80±0.64	11.60±0.58	12.48±0.62

The values of thermal diffusivity and thermal conductivity of the ceramic samples studied, in the whole, reduced as the temperature rises (Fig. 7, *a*, *b*) and unmonotonously changed with increasing of substitution degree of calcium by bismuth in $Ca_3Co_4O_{9+\delta}$: for the single-phase samples values of η and λ increased at x increasing, but for non-single-phase samples they decreased at x increasing (Fig. 7, *c*, *d*). The first is, probably, caused by decreasing of $Ca_3Co_4O_{9+\delta}$-based ceramics porosity at doping its by Bi_2O_3, but second is due to the increasing of density of interphases in the heterogeneous ceramics, serving as effective areas of phonon scattering. It is noted that the lowest thermal diffusivity values were demonstrated by $Ca_{2.4}Bi_{0.6}Co_4O_{9+\delta}$ composite, whereas the lowest values of thermal conductivity among the samples studied were possessed by the matrix phase – undoped layered calcium cobaltite, which is, probably, caused by the most values of its porosity.

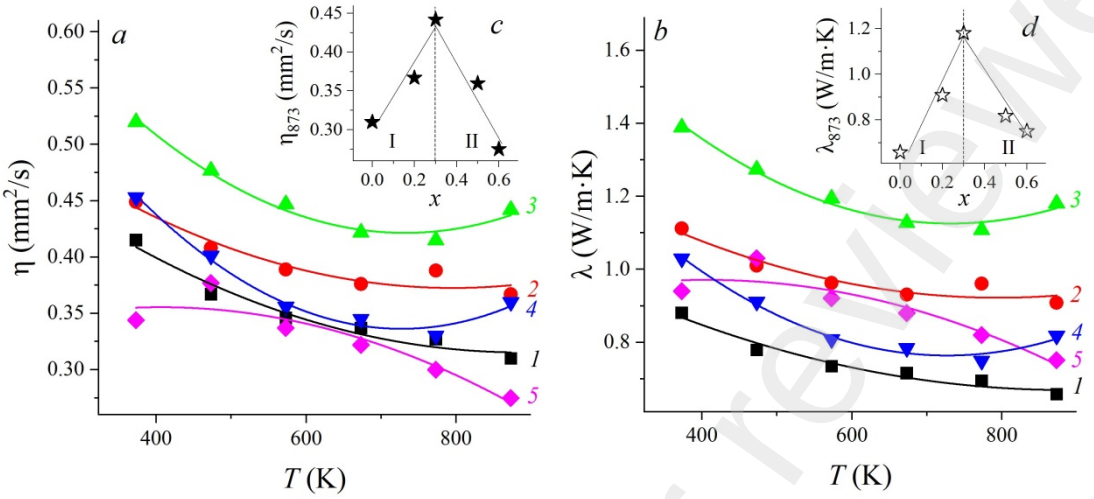

Fig. 7. Temperature (*a*, *b*) and concentration (*c*, *d*) dependences of thermal diffusivity (η) (*a*, *c*) and thermal conductivity (λ) (*b*, *d*) of the $Ca_{3-x}Bi_xCo_4O_{9+\delta}$ sintered ceramics: x = 0.0 (*1*), 0.2 (*2*), 0.3 (*3*), 0.5 (*4*), and 0.6 (*5*). I – single-phase region, II – non-single-phase region

The electronic part of the thermal conductivity of the studied materials increased nearly linearly with increasing of temperature and was about 1.3–5.6% and 5.2–18.8% of the total thermal conductivity of the samples at 373 K and 873 K, respectively (Fig. 8, *a*). The phonon part of the thermal conductivity was dominating and, in the whole, decreased with increasing of temperature (Fig. 8, *b*). Increasing of substitution degree of Ca^{2+} by Bi^{3+} results in increasing of λ_{el}, which was more pronounced for single-phase samples (Fig. 8, *c*). With x increasing, λ_{ph} changed by the same way, as total thermal conductivity; hereby, the least value of phonon part of thermal

conductivity was found for $Ca_{2.4}Bi_{0.6}Co_4O_{9+\delta}$ compound – 0.61 W/(m·K) at 873 K (Fig. 8, *d*).

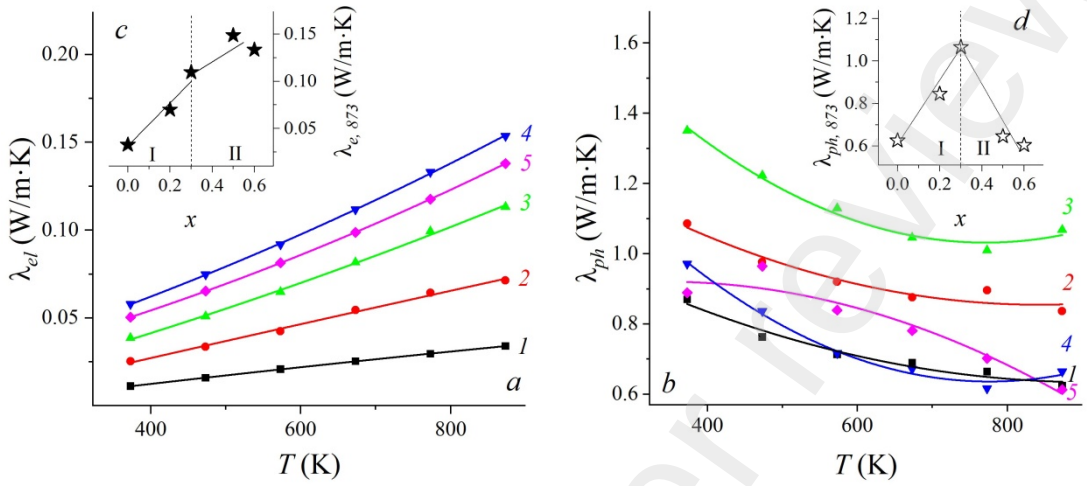

Fig. 8. Temperature (*a*, *b*) and concentration (*c*, *d*) dependences of electron (λ_{el}) (*a*, *c*) and phonon (λ_{ph}) parts (*b*, *d*) of thermal conductivity of $Ca_{3-x}Bi_xCo_4O_{9+\delta}$ samples: x = 0.0 (*1*), 0.2 (*2*), 0.3 (*3*), 0.5 (*4*), and 0.6 (*5*). I – single-phase samples, II – non-single-phase samples

3.5. Functional (thermoelectric) properties

The power factor values of obtained ceramic samples increased with temperature nearly linearly and with increasing of bismuth oxide content in the samples, hereby the most pronounced increase was found for the single-phase region (Fig. 9). The highest power factor of 284 $\mu W \cdot m^{-1} \cdot K^{-2}$ at 1073 K was found for the composite $Ca_{2.4}Bi_{0.6}Co_4O_{9+\delta}$ ceramics consisting of $Ca_{2.7}Bi_{0.3}Co_4O_{9+\delta}$ solid solution and $Bi_2Ca_2Co_{1.7}O_y$ phase, which was 4.6 times larger than for the parent $Ca_3Co_4O_{9+\delta}$ phase having the same thermal prehistory.

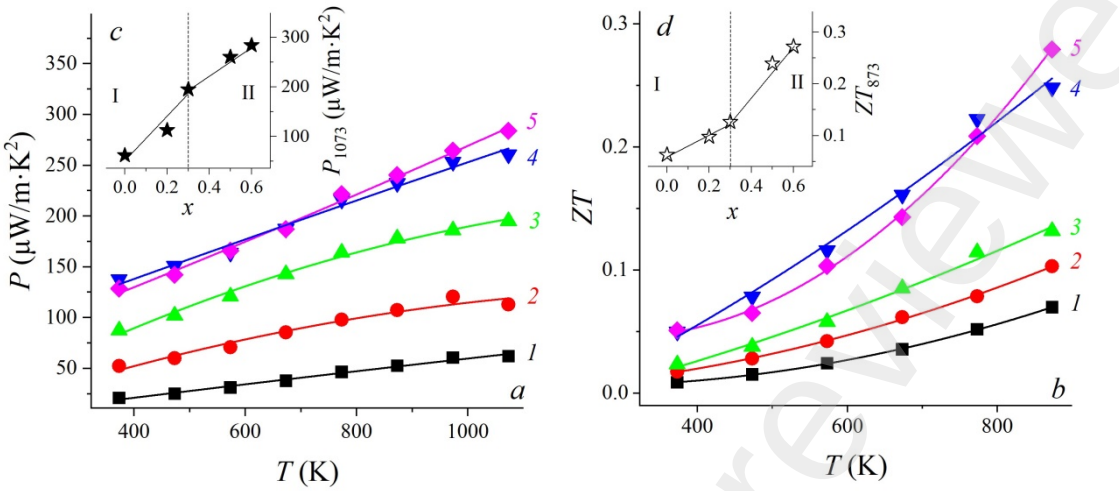

Fig. 9. Temperature (*a*, *b*) and concentration (*c*, *d*) dependences of power factor (*P*) (*a*, *c*) and figure-of-merit (*ZT*) (*b*, *d*) of $Ca_{3-x}Bi_xCo_4O_{9+\delta}$ oxide thermoelectrics: x = 0.0 (*1*), 0.2 (*2*), 0.3 (*3*), 0.5 (*4*), and 0.6 (*5*). I – homogeneous ceramics, II – composite ceramics

The figure-of-merit (*ZT*) values of the samples also increased with the increasing of temperature (Fig. 9) and substitution degree of calcium by bismuth, but in the last case the most pronounced increase was observed in the non-single-phase region (Fig. 9). The largest *ZT* value was detected for $Ca_{2.4}Bi_{0.6}Co_4O_{9+\delta}$ compound – 0.279 at 873 K, which was 4.0 times larger than for the parent $Ca_3Co_4O_{9+\delta}$ phase with similar thermal prehistory.

In the Table 4 are summarized the main characteristics of ceramics obtained in this work and possessing the best thermoelectric performance comparing with the literature data on $Ca_3Co_4O_{9+\delta}$-based ceramics having different composition and prepared by various methods. As can be seen, thermoelectric material obtained in this work possesses a relatively low power factor value due to its high electrical resistivity caused by high porosity value of the sample.

Table 4. Literature-reported functional characteristics of $Ca_3Co_4O_{9+\delta}$-based ceramics comparing with the results reported in this study

Formula	Synthesis method	Sintering method	Measurement temperature, K	ρ, μΩ·m	*S*, μV/K	*P*, μW/m·K²	λ, W/m·K	*ZT*	Year	Ref
$Ca_{2.5}Bi_{0.5}Co_4O_{9+\delta}$	SSR	CS	973	95	160	270	1.34	0.2	2000	[17]
$Ca_{2.85}Bi_{0.15}Co_4O_{9+\delta}$	Sol-gel	SPS	973	69	179	461	1.81	0.25	2008	[45]
$Ca_{2.9}Bi_{0.1}Co_4O_{9+\delta}$ (air) $Ca_{2.85}Bi_{0.15}Co_4O_{9+\delta}$ (air) $Ca_{2.8}Bi_{0.2}Co_4O_{9+\delta}$ (Ar) $Ca_{2.8}Bi_{0.2}Co_4O_{9+\delta}$ (air)	SSR	HP + post annealing at 973 K (on air or Ar)	870 870 870 870	87 98 189 118	160 171 197 170	294 298 206 246	– – 1.16 –	0.16 0.18 0.15 0.19	2011	[48]
$Ca_{2.7}Bi_{0.3}Co_{3.9}Fe_{0.1}O_{9+\delta}$	SSR	SPS	973	74	182	451	1.18	0.4	2014	[18]
$Ca_3Co_4O_{9+\delta}$ / 10 wt % Ag	Sol-gel	TSS	1073	100	210	430	–	–	2015	[33]
$Ca_{2.9}Cd_{0.1}Co_4O_{9+\delta}$ / 10 wt % Ag	SSR	HP	952	41	189	880	2.72	0.31	2019	[9]
$Ca_3Co_4O_{9+\delta}$ / 2 wt % Cu	GCN process	HP	1100	87	211	521	–	0.223	2020	[34]
$Ca_3Co_4O_{9+\delta}$ / 0.05 wt % SiC	SSR	CS	923	105	195	365	1.54	0.218	2020	[37]
$Ca_{2.7}Bi_{0.3}Co_{3.92}O_{9+\delta}$	SSR	SPS + post annealing at 1023 K	823	80	160	340	1.79	0.16	2020	[57]
$Ca_3Co_4O_{9+\delta}$ / 0.75 wt % TiC $Ca_3Co_4O_{9+\delta}$ / 0.25 wt % TiC	SSR	CS	1073 1073	145 170	195 194	262 222	1.82 1.47	0.15 0.16	2021	[38]
$Ca_{2.4}Bi_{0.6}Co_4O_{9+\delta}$	SSR	CS	1073 873	156	211	284 240	0.75	0.28	2025	This work

SSR – solid state reaction; GCN process – glycine-citrate-nitrate process; CS – conventional sintering; SPS – spark-plasma sintering; HP – hot pressing; TSS – two-step sintering

The low thermal conductivity value of ceramics studied, which results in the high value of its figure-of-merit is close to the *ZT* values reported in the literature for $Ca_3Co_4O_{9+\delta}$-based ceramic doped with silver or iron samples with the best thermoelectric performance [9,18]. It can be expected that using of special synthesis and sintering techniques enables synthesis of low-porous $(Ca,Bi)_3Co_4O_{9+\delta}$ composite ceramic with improved thermoelectric efficiency, similar to single-phase $Ca_{2.7}Bi_{0.3}Co_4O_{9+\delta}$ material reported in [57]. Lowering of ceramics porosity along with decreasing of its grain sizes should result in increasing of its Seebeck coefficient and decreasing of electrical resistivity and thermal conductivity which should lead essential improve of ceramics thermoelectric efficiency. The effectiveness of proposed approach will be checked due to the further experiments.

4. Conclusions

Doping of layered calcium cobaltite ceramics with bismuth oxide results in improving of its sinterability and texturing degree which is more pronounced for composite samples containing besides the $Ca_{2.7}Bi_{0.3}Co_4O_{9+\delta}$ solid solution the second phase of layered bismuth–calcium cobaltite $Bi_2Ca_2Co_{1.7}O_y$. Lowering of ceramics porosity results in decreasing of its electrical resistivity, which values are minimal for the $Ca_{3-x}Bi_xCo_4O_{9+\delta}$ (x = 0.5, 0.6) compounds – 152–156 μΩm at 1073 K which is 3.8 times lower than for base layered calcium cobaltite. Formation of phase inhomogeneity in ceramics results in improving of its Seebeck coefficient, which reaches the maximal value for $Ca_{2.4}Bi_{0.6}Co_4O_{9+\delta}$ compound – 210 μV/K at 1073 K which is 9% larger than for parent calcium cobaltite. Thermal conductivity values of ceramics at bismuth oxide doping increased for single-phase materials due to decreasing of their porosity and

decreased for composite ones due to increasing of phase interfaces serving as additional phonon scattering sites.

The largest thermoelectric efficiency among the studied samples possesses $Ca_{2.4}Bi_{0.6}Co_4O_{9+\delta}$ composite ceramics, which power factor and figure-of-merit values are of 284 $\mu W \cdot m^{-1} \cdot K^{-2}$ (at 1073 K) and 0.279 (at 873 K), those are 4.6 and 4 times higher than for base layered calcium cobaltite and are provided by both low resistivity and high Seebeck coefficient values of this compound due to its less porosity and phase inhomogeneity.

Obtained results show the effectiveness of bismuth oxide doping strategy in improving the thermoelectric efficiency of $Ca_3Co_4O_{9+\delta}$-based ceramics, which can be further improved due to the using of special sintering methodic and variation of its thermal prehistory.

CRediT authorship contribution statement

Klyndyuk Andrei I.: Conceptualization, Methodology, Supervision, Project administration, Funding acquisition, Validation, Resources, Data Curation, Writing – Original Draft, Writing – Review &Editing. **Matsukevich Iryna V.:** Funding acquisition, Validation, Formal analysis, Investigation, Resources, Writing – Original Draft. **Latypov Roman S.:** Validation, Data Curation, Formal analysis, Visualization, Writing – Original Draft. **Chizhova Ekaterina A.:** Visualization, Validation, Formal analysis, Investigation, Data Curation. **Veteška Peter:** Formal analysis, Investigation, Resources. **Ondrej Hanzel:** Formal analysis, Investigation, Resources. **Janek Marián:** Supervision, Project administration, Funding acquisition, Resources, Writing – Review &Editing.

Declaration of competing interest

The authors declare that they have no known competing financial interests or personal relationships that could have appeared to influence the work reported in this paper.

Data availability

The raw/processed data required to reproduce the findings of this study are available from the corresponding authors upon request.

Acknowledgements

Andrei I. Klyndyuk and Ekaterina A. Chizhova acknowledge financial support by the Ministry of Education of the Republic of Belarus (State Research Program "Functional and Engineering Materials and Technologies, Nanomaterials and Nanotechnologies in Modern Technology (Functional and Engineering Materials, Nanomaterials", subprogram "Crystal and Molecular Structures", complex task "Development and Study of New Efficient Ferroelectromagnetics (Multiferroics) with a Giant Magnetoelectric Effect Based on Solid Solutions of Bismuth Ferrite and Promising Thermoelectrics Based on Layered Cobaltites"). Iryna V. Matsukevich acknowledges financial support by the National Scholarship Program of the Slovak Republic and European Union Horizon 2020 Research and Innovation Program under grant agreement No. 739566. Marián Janek acknowledges the financial support by the Slovak Scientific Grant Agency (grants VEGA No. 1/0070/22. Ondrej Hanzel acknowledges the financial support by the Slovak Scientific Grant Agency (grant VEGA No. 2/0094/25) and Slovak Research and Development Agency, Contract No. APVV-24-0442. This work was funded by the EU Next Generation EU through the Recovery and Resilience Plan for Slovakia under the project No. 09I03-03-V03-00094/2024/VA.

Appendix A. Supporting Information

Supplementary data associated with this article can be found in the online version at doi:10.1016/j.jeurceramsoc.2025.000000.

References

[1] Y. Zhou, L.–D. Zhao, Promising Thermoelectric Bulk materials with 2D Structures, Adv. Mater. 29 (2017) 1702676. https://doi.org/10.1002/adma.201702676.

[2] K. Koumoto, R. Funuhashi, E.Guilmeau, Y. Miyazaki, A. Weidenkaff, Y. Wang, C. Wan, Thermoelectric Ceramics for Energy Harvesting, J. Am. Ceram. Soc. 96 (2013) 1–23. https://doi.org/10.1111/jace.12076.

[3] E.I.Konstantinova, V.A.Litvinov, M.A.Ryzhkov, A.D.Koryakov, I.A.Leonidov, Thermoelectric properties of $Ca_{0.5-x}Sr_{0.5}Lu_xMnO_{3-\delta}$ Manganites, Inorg. Mater. 59 (2023) 1319–1325. https://doi.org/10.1134/S0020168523120051.

[4] K. Fujimoto, M.Gibu, Y. Yamaguchi, F.Fimi, K. Nishio, J. Rabin, I. Takeuchi, Thermoelectric properties of bismuth-substituted calcium manganite $Ca_{1-x}Bi_xMnO_{3-\delta}$ prepared via the electrostatic spray deposition method, J. Ceram. Soc. Jpn. 125 (2017) 308–312. https://doi.org/10.2109/jcersj2.16277.

[5] J.H. Lin, C.S. Hwang, F.R. Sie, Preparation and thermoelectric properties of Nd and Dy co-doped $SrTiO_3$ bulk materials, Mater. Res. Bull. 122 (2020) 110650. https://doi.org/10.1016/j.materresbull.2019.110650.

[6] P. Cao, J. Yao, Y. Sun, A.I. Klyndyuk, Z. Li, A. Abbas, N.S. Krasutskaya, W. Su, C. Wang, H. Wang, Optimized configuration entropy for synergistic enhancement of thermoelectric performance for $SrTiO_3$-based ceramics, J. Eur. Ceram. Soc. 45 (2025) 117290. https://doi.org/10.1016/j.jeurceramsoc.2025.117290.

[7] W. Zhang, K. Zhu, J. Liu, J. Wang, K. Yan, P. Liu, Y. Wang, Influence of the phase transformation in Na_xCoO_2 ceramics on thermoelectric properties, Ceram. Int. 44 (2018) 17251–17257. https://doi.org/10.1016/j.ceramint.2018.06.183.

[8] N.S. Krasutskaya, A.I. Klyndyuk, L.E. Evseeva, N.N. Gundilovich, E.A. Chizhova, A.V. Paspelau, Enhanced Thermoelectric Performance of $Na_{0.55}CoO_2$ Ceramics Doped by Transition and Heavy Metal Oxides, Solids. 5 (2024) 267–277. https://doi.org/10.3390/solids5020017.

[9] W. Li, J. Wang, B. Poudel, H.B. Kang, S. Huxtable, A. Nozariasbmarz, U. Saparamadu, S. Priya, Filiform metal silver nanoinclusions to enhance thermoelectric performance of *p*-type $Ca_3Co_4O_{9+\delta}$ oxide, ACS Appl. Mater. & Interfaces. 11 (2019) 42131–42138. https://doi.org/10.1021/acsami.9b13607.

[10] A.I. Klyndyuk, D.S. Kharytonau, I.V. Matsukevich, E.A. Chizhova, Z. Lenčéš, R.P. Socha, M. Zimowska, O. Hanzel, M. Janek, Effect of cationic nonstoichiometry on thermoelectric properties of layered calcium cobaltite obtained by field assisted sintering technology (FAST), Ceram. Int. 50 (2024) 30970–30979. https://doi.org/10.1016/j.ceramint.2024.05.402.

[11] A. Sotelo, S. Rasekh, M.A. Madre, E. Guilmeau, S. Marinel, J.C. Diez, Solution-based synthesis routes to thermoelectric $Bi_2Ca_2Co_{1.7}O_x$, J. Eur. Ceram. Soc. 31 (2011) 1763–1769. https://doi.org/10.1016/j.jeurceramsoc.2011.03.008.

[12] A.I. Klyndyuk, N.S. Krasutskaya, A.A. Khort, Synthesis and properties of ceramics based on a layered bismuth calcium cobaltite, Inorg. Mater. 54(2018) 509–514. https://doi.org/10.1134/S0020168518050059.

[13] A.C. Masset, C. Michel, A. Maignan, M. Hervieu, O. Toulemonde, F. Studer, B. Raveau, Misfit-layered cobaltite with an anisotropic giant magnetoresistance: $Ca_3Co_4O_9$, Phys. Rev. B. 62 (2000) 166–175. https://doi.org/10.1103/PhysRevB.62.166.

[14] J.W. Fergus, Oxide materials for high temperature thermoelectric energy conversion, J. Eur. Ceram. Soc. 32 (2012) 525–540. https://doi.org//10.1016/j.jeurceramsoc.2011.10.007.

[15] M. Prevel, O. Perez, J.G. Noudem, Bulk textured $Ca_{2.5}(RE)_{0.5}Co_4O_9$ (RE: Pr, Nd, Eu, Dy and Yb) thermoelectric oxides by sinter-forging, Solid State Sci. 9 (2007) 231–235. https://doi.org/10.1016/j.solidstatesciences.2007.01.003.

[16] A.I. Klyndyuk, I.V. Matsukevich, Synthesis and properties of $Ca_{2.8}Ln_{0.2}Co_4O_{9+\delta}$ (Ln = La, Nd, Sm, Tb-Er) solid solutions, Inorg. Mater. 48 (2012) 1052–1057. https://doi.org/10.1134/S0020168512090099.

[17] S. Li, R. Funahashi, I. Matsubara, K. Ueno, S. Sodeoka, H. Yamada, Synthesis and Thermoelectric Properties of the New Oxide Materials $Ca_{3-x}Bi_xCo_4O_{9+\delta}$ ($0.0 < x < 0.75$), Chem. Mater. 12 (2000) 2424–2427. https://doi.org/10.1021/cm000132r.

[18] R. Tian, T. Zhang, D. Chu, R. Donelson, L. Tao, S. Li, Enhancement of high temperature thermoelectric performance in Bi, Fe co-doped layered oxide-based material $Ca_3Co_4O_{9+\delta}$, J. Alloys Compd. 615 (2014) 311–315. https://doi.org/10.1016/j.jallcom.2014.06.190.

[19] I.V. Matsukevich, A.I. Klyndyuk, E.A. Tugova, A.N. Kovalenko, A.A. Marova, N.S. Krasutskaya, Thermoelectric properties of $Ca_{3-x}Bi_xCo_4O_{9+\delta}$ ($0.0 \le x \le 1.5$) ceramics, Inorg. Mater. 52 (2016) 593–599. https://doi.org/10.1134/S0020168516060091.

[20] S. Demirel, E. Altin, E. Oz, S. Altin, A. Bayri, An enhancement *ZT* and spin state transition of $Ca_3Co_4O_9$ with Pb doping, J. Alloys Compd. 627 (2015) 430–437. https://doi.org/10.1016/j.jallcom.2014.11.200.

[21] A.I. Klyndyuk, I.V. Matsukevich, Synthesis, Structure, and Properties of $Ca_3Co_{3.85}M_{0.15}O_{9+\delta}$ (M = Ti–Zn, Mo, W, Pb, Bi) Layered Thermoelectrics, Inorg. Mater. 51 (2015) 944–950. https://doi.org/10.1134/S0020168515080105.

[22] S. Neelakandan, K. Biswas, Tweaking the interplay of the layers by substitution in $Ca_3Co_4O_{9+\delta}$ for high efficiency thermoelectric materials, J. Alloys Compd. 971 (2024) 172693. https://doi.org/10.1016/j.jallcom.2023.172693.

[23] S. Katsuyama, Y. Takiguchi, M. Ito, Synthesis of $Ca_3Co_4O_9$ ceramics by polymerized complex and hydrothermal hot-pressing processes and the investigation of its thermoelectric properties, J. Mater. Sci. 43 (2008) 3553–3559. https://doi.org/10.1007/s10853-008-2561-x.

[24] A.K. Królicka, M. Piersa, A. Mirowska, M. Michalska, Effect of sol-gel and solid-state synthesis techniques on structural, morphological and thermoelectric performance of $Ca_3Co_4O_9$, Ceram. Int. 44 (2018) 13736–13743. https://doi.org/10.1016/j.ceramint.2018.04.215.

[25] S. Lin, J. Selig, Self-propagating High-temperature Synthesis of $Ca_{1.24}Co_{1.62}O_{3.86}$ Thermoelectric Powders, J. Alloys Compd. 503 (2010) 402–409. https://doi.org/10.1016/j.jallcom.2010.05.018.

[26] S. Bresch, B. Mieller, D. Schönauer-Kamin, R. Moos, T. Reimann, F. Giovannelli, T. Rabe, Influence of pressure and dwell time on pressure-assisted sintering of calcium cobaltite, J. Am. Ceram. Soc. 104 (2021) 917–927. https://doi.org/10.1111/jace.17541.

[27] N. Kanas, S.P. Singh, M. Rotan, M. Saleemi, M. Bittner, A. Feldhoff, T. Norby, K. Wiik, T. Grande, M.A. Einarsrud, Influence of processing on stability, microstructure and thermoelectric properties of $Ca_3Co_{4-x}O_{9+\delta}$, J. Eur. Ceram. Soc. 38 (2018) 1592–1599.https://doi.org/10.1016/j.jeurceramsoc.2017.11.011.

[28] X. Li, J. Wu, S. Huang, Y. Gao, D. Liu, J. Liu, H.T. Lin, Enhancing thermoelectric properties of $Ca_3Co_4O_9$ ceramics through oscillatory pressure sintering, J. Mater. Res. Technol. 28 (2024) 3475–3484. https://doi.org/10.1016/j.jmrt.2023.12.256.

[29] T. Schulz, J. Töpfer, Thermoelectric properties of $Ca_3Co_4O_9$ ceramics prepared by an alternative pressure-less sintering/annealing method, J. Alloys Compd. 659 (2016) 122–126. https://doi.org/10.1016/j.jallcom.2015.11.001.

[30] A.I. Klyndyuk, E.A. Chizhova, E.A. Tugova, R.S. Latypov, O.N. Karpov, M.V. Tomkovich, Thermoelectric multiphase ceramics based on layered calcium cobaltite, as synthesized using two-stage sintering, GlassPhys. Chem. 46 (2020) 562–569. https://doi.org/10.1134/S1087659620060127.

[31] A.I. Klyndyuk, E.A. Chizhova, R.S. Latypov, S.V. Shevchenko, V.M. Kononovich, Effect of the Addition of Copper Particles on the Thermoelectric Properties of the $Ca_3Co_4O_{9+\delta}$ Ceramics Produced by Two-step Sintering, Russ. J. Inorg. Chem. 67 (2022) 237–244. https://doi.org/10.1134/S0036023622020073.

[32] P.H. Xiang, Y. Kinemuchi, H. Kaga, K. Watari, Fabrication and thermoelectric properties of $Ca_3Co_4O_9$/Ag composites, J. Alloys Compd. 454 (2008) 364–369. https://doi.org/10.1016/j.jallcom.2006.12.102.

[33] F. Kahraman, M.A. Madre, S. Rasekh, C. Salvador, P. Bosque, M.A. Torres, J.C. Diez, A. Sotelo, Enhancement of mechanical and thermoelectric properties of $Ca_3Co_4O_9$ by Ag addition, J. Eur. Ceram. Soc. 35 (2015) 3835–3841. https://doi.org/http://dx.doi.org/10.1016/j.jeurceramsoc.2015.05.029.

[34] A.I. Klyndyuk, I.V. Matsukevich, M. Janek, E.A. Chizhova, Z. Lenčéš, O. Hanzel, P. Veteška, Effect of copper additions on the thermoelectric properties of

a layered calcium cobaltite prepared by hot pressing, Inorg. Mater. 56 (2020) 1198–1205. https://doi.org/10.1134/S0020168520110059.

[35] F. Delorme, P. Diaz-Chao, E. Guilmeau, F. Giovannelli, Thermoelectric properties of $Ca_3Co_4O_9$–Co_3O_4 composites, Ceram. Int. 41 (2015) 10038–10043. https://doi.org/10.1016/j.ceramint.2015.04.091.

[36] R.K. Gupta, R. Sharma, A.K. Mahapatro, R.P. Tandon, The effect of ZrO_2 dispersion on the thermoelectric power factor of $Ca_3Co_4O_9$, Phys. B: Condens. Matter. 483 (2016) 48–53. https://doi.org/10.1016/j.physb.2015.12.028.

[37] C. Ruan, H. Song, M. Fan, H. Hao, S. Liu, Enhancement of $Ca_3Co_4O_{9+\delta}$ thermoelectric properties by dispersing SiC nanoparticles, Ceram. Int. 47 (2021) 6548–6553. https://doi.org/10.1016/j.ceramint.2020.10.242.

[38] H. Amaveda, O.J. Dura, M. Mora, M.A. Torres, G. Guelou, M.A. Madre, S. Marinel, A. Sotelo, Tuning $Ca_3Co_4O_9$ thermal and transport properties by TiC nanoparticles addition, Boletín de la Soc. Española de Cerámica y Vidr. 60 (2021) 138–146. https://doi.org/10.1016/j.bsecv.2020.03.006.

[39] P. Carvillo, Y. Chen, C. Boyle, P.N. Barnes, X. Song, Thermoelectric performance enhancement of calcium cobaltite through barium grain boundary segregation, Inorg. Chem. 54 (2015) 9027–9032. https://doi.org/10.1021/acs.inorgchem.5b01296.

[40] P. Zhang, Z. Lou, L. Gong, J. Xu, Q. Chen, M.J. Reece, H. Yan, Z. Dashevsky, F. Gao, High-entropy $MTiO_3$ perovskite oxides with glass-like thermal conductivity for thermoelectric applications, J. Alloys Compd. 937 (2023) 168366. https://doi.org/10.1016/j.jallcom.2022.168366.

[41] Y. Zhu, X. Liu, M.A. Buckingham, P. Acharyya, E. Guilmeau, B.L. Mehdi, D.J. Lewis, R. Freer, Ultra-low thermal conductivity in a perovskite oxide thermoelectric through entropy engineering, J. Eur. Ceram. Soc. 44 (2024) 4666–4679. https://doi.org/10.1016/j.jeurceramsoc.2024.02.022.

[42] C. Yang, H. Wu, H. Song, X. Wang, S. Chen, X. Xu, L. Chen, Z. Zhao, L. Yu, B. Liu, Ultralow thermal conductivity and enhanced thermoelectric properties in a textured $(Ca_{0.35}Sr_{0.2}Ba_{0.15}Na_{0.2}Bi_{0.1})_3Co_4O_9$ high-entropy ceramic, J. Alloys Compd. 940 (2023) 168802. https://doi.org/10.1016/j.jallcom.2023.168802.

[43] G. Xu, R. Funahashi, M. Shikano, I. Matsubara, Y. Zhou, Thermoelectric properties of the Bi- and Na-substituted $Ca_3Co_4O_9$ system, Appl. Phys. Lett. 80 (2002) 3760–3762. https://doi.org/10.1063/1.1480115.

[44] Y. Miyazaki, Y. Suzuki, M. Onoda, Y. Ishii, Y. Morii, T. Kajitani, Modulated structure of misfit layered cobalt oxide $[(Ca_{0.90}Bi_{0.10})_2(Co_{0.95}Bi_{0.05})O_3]_pCoO_2$, Jpn. J. Appl. Phys. 43 (2004) 6252. https://doi.org/10.1143/JJAP.43.6252.

[45] Y. Liu, Y. Lin, L. Jiang, C.W. Nan, Z. Shen, Thermoelectric properties of Bi^{3+} substituted Co-based misfit-layered oxides, J. Electroceramics. 21 (2008) 748–751. https://doi.org/10.1007/s10832-007-9297-x.

[46] J.W. Park, D.H. Kwak, S.H. Yoon, S.C. Choi, Thermoelectric properties of highly oriented $Ca_{2.7}Bi_{0.3}Co_4O_9$ fabricated by rolling process, J. Ceram. Soc. Jpn. 117 (2009) 643–646. https://doi.org/http://dx.doi.org/10.2109/jcersj2.117.643.

[47] T. Sun, H.H. Hng, Q.Y. Yan, J. Ma, Enhanced high temperature thermoelectric properties of Bi-doped *c*-axis oriented $Ca_3Co_4O_9$ thin films by pulsed laser deposition, J. Appl. Phys. 108 (2010) 083709. https://doi.org/10.1063/1.3499324.

[48] D. Moser, L. Karvonen, S. Populoh, M. Trottmann, A. Weidenkaff, Influence of the oxygen content on thermoelectric properties of $Ca_{3-x}Bi_xCo_4O_{9+\delta}$ system, Solid State Sci. 13 (2011) 2160–2164. https://doi.org/http://dx.doi.org/10.1016/j.solidstatesciences.2011.10.001.

[49] J.Y. Cho, O.J. Kwon, Y.K. Chung, J.S. Kim, W.S. Kim, K.J. Song, C. Park, Effect of trivalent Bi doping on the Seebeck coefficient and electrical resistivity of $Ca_3Co_4O_9$, J. Electron. Mater. 44 (2015) 3621–3626. https://doi.org/10.1007/s11664-015-3924-0.

[50] I.V. Matsukevich, A.I. Klyndyuk, E.A. Tugova, M.V. Tomkovich, N.S. Krasutskaya, V.V. Gusarov, Synthesis and properties of materials based on layered calcium and bismuth cobaltites, Russ. J. Appl. Chem. 88 (2015) 1241–1247. https://doi.org/10.1134/S1070427215080030.

[51] A.I. Klyndyuk, I.V. Matsukevich, Synthesis and properties of disubstituted derivatives of layered calcium cobaltite, Glass Phys. Chem. 41 (2015) 545–550. https://doi.org/10.1134/S1087659615050077.

[52] C. Boyle, P. Carvillo, Y. Chen, E.J. Barbero, D. McIntyre, X. Song, Grain boundary segregation and thermoelectric performance enhancement of bismuth doped calcium cobaltite, J. Eur. Ceram. Soc. 36 (2016) 601–607. https://doi.org/10.1016/j.jeurceramsoc.2015.10.042.

[53] C. Boyle, L. Liang, Y. Chen, J. Prucz, E. Cakmak, T.R. Watkins, E. Lara-Curzio, X. Song, Competing dopants grain boundary segregation and resultant Seebeck coefficient and power factor enhancement of thermoelectric calcium cobaltite ceramics, Ceram. Int. 43 (2017) 11523–11528. https://doi.org/10.1016/j.ceramint.2017.06.029.

[54] J. Wang, Q. Chen, X.C. Zhu, S.J. Lee, K.W. Park, C.Y. Jhun, Preparation and thermoelectric properties of Bi doped $Ca_3Co_4O_9$ based thermoelectric materials, Key Eng. Mater. 783 (2018) 144–147. https://doi.org/10.4028/www.scientific.net/KEM.783.144.

[55] M.M. Mohammed, S. Izman, M.N. Alias, R. Srithaer, M.B. Uday, H.O. Noor, F.O. Muhammad, Investigation on microstructure and electrical properties of Bi doping $Ca_3Co_4O_9$ nanoparticles synthesized by sol-gel process, Int. J. Eng. & Technol. 7 (2018) 31–33. https://doi.org/10.14419/ijet.v7i2.29.13121.

[56] S. Bresch, B. Mieller, D. Schoenauer-Kamin, R. Moos, F. Giovanelli, T. Rabe, Influence of pressure assisted sintering and reaction sintering on microstructure and thermoelectric properties of Bi-doped and undoped calcium cobaltite, J. Appl. Phys. 126 (2019) 075102. https://doi.org/10.1063/1.5107476.

[57] J. Yu, K. Chen, F. Azough, D.T. Alvarez-Ruiz, M.J. Reece, R. Freer, Enhancing the thermoelectric performance of calcium cobaltite ceramics by tuning composition and processing, ACS Appl. Mater. & Interfaces. 12 (2020) 47634–47646. https://doi.org/10.1021/acsami.0c14916.

[58] J. Yu, Y. Chang, E. Jakubczyk, B. Wang, F. Azough, R. Dorey, R. Freer, Modulation of electrical transport in calcium cobaltite ceramics and thick films through microstructure control and doping, J. Eur. Ceram. Soc. 41 (2021) 4859–4869. https://doi.org/10.1016/j.jeurceramsoc.2021.03.044.

[59] A.I. Klyndyuk, N.S. Krasutskaya, I.V. Matsukevich, E.A. Tugova, E.A. Chizhova, Phase equilibria in the $BiO_{1.5}$–CaO–CoO_y system, Russ. J. Gen. Chem. 88 (2018) 1063–1065. https://doi.org/10.1134/S1070363218060014

[60] L. Speichalova, O. Jankovsky, K. Rubesova, V. Jakes, A.–M. Lauermannova, D. Sedmidubsky, Solid-Liquid Equilibria in the Bi–Ca–Co–O System, J. Eur. Ceram. 42 (2022) 5756–5761. https://doi.org/10.1016/j.jeurceramsoc.2022.06.064

[61] R. Funahashi, S. Urata, Fabrication and application of an oxide thermoelectric System, Int. J. Appl. Ceram. Technol. 4 (2007) 297–307. https://doi.org/10.1111/j.1744-7402.2007.02144.x.

[62] O.V. Merkulov, B.V. Politov, K.Y. Chesnokov, A.A. Markov, I.A. Leonidov, M.V. Patrakeev, Fabrication and testing of a tubular thermoelectric module based on oxide elements, J. Electron. Mater. 47 (2018) 2808–2816. https://doi.org/10.1007/s11664-018-6150-8.

[63] A. Bochmann, T. Reimann, T. Schulz, S. Teichert, J. Töpfer, Transverse thermoelectric multilayer generator with bismuth-substituted calcium cobaltite: design optimization through variation of tilt angle, J. Eur. Ceram. Soc. 39 (2019) 2923–2929. https://doi.org/10.1016/j.jeurceramsoc.2019.03.036.

[64] A.I. Goryachko, S.N. Ivanin, V.Yu Buz'ko, Synthesis, microstructural and electromagnetic characteristics of cobalt-zinc ferrite, Kondensirovannye Sredy I Mezhfaznye Granitsy = Condensed Matter and Interphases. 22 (4) (2020) 446–452. https://doi.org/10.17308/kcmf.2020.22/3115.

[65] C.U. Nikam, S.R. Kadam, R.S. Shitole, A.P. Birajdar, V.K. Barote, S.R. Wadgnae, R. H. Kadam, R.G. Kale, Williamson–Hall and Size–strain plot based micro-structural analysis and evaluation of elastic properties of Dy^{3+} substituted Co–Zn nano-spinels, J. Phys. Conf. Ser. 2426 (2023) 012029. https://doi.org/10.1088/17426596/2426/1/012029.

[66] Y.T. Prabhu, K.V. Rao, V.S.S. Kumar, B.S. Kumari, X-ray analysis by Williamson–Hall and size–strain plot methods of ZnO nanoparticles with fuel variation, World J. Nano Sci. Eng. 4 (1) (2014) 21–28. https://doi.org/10.4236/wjnse.2014.41004.

[67] F.K. Lotgering, Topotactical reactions with ferrimagnetic oxides having hexagonal crystal structures—I, J. Inorg. Nucl. Chem. 9 (1959) 113–123. https://doi.org/10.1016/0022-1902(59)80070-1.

[68] M. Torki, B. Mohavedi, S. Ghazanfari, M. Milani, Fabrication and mechanical characterization of YAG ceramic-composite with alumina nanoparticles using slip casting and sintering process, Mater. Res. Express. 7 (2000) 115010. https://doi.org/10.1088.2053-1591/abca6b.

[69] G.J.Snyder, A.H.Snyder, M.Wood, R.Gurunathan, B.H.Snyder, C.Niu, Weighted Mobility, Adv. Mater. 32 (25) (2020) 2001537. https://doi.org/10.1002/adma.202001537.

[70] R.D. Shannon, C.T. Prewitt, Effective ionic radii in oxides and fluorides, Acta Crystallogr. Sect. B Struct. Crystallogr. Cryst. Chem. 25 (1969) 925–946. https://doi.org/10.1107/S0567740869003220.

[71] L.Pan, S.Mitra, L.-D.Zhao, Ya.Shen, Yi.Wang, Cl.Fesel, D.Berardan, The Role of Ionized Impurity Scattering on the Thermoelectric Performances of Rock Salt $AgPb_mSnSe_{2+m}$,Adv. Funct. Mater. 26 (2016) 5149–5157. https://doi.org/10.1002/adfm.201600623.

[72] Y.-H. Lin, J. Lan, Z. Shen, Y. Liu, C.-W. Nan, J.-F. Li, High-temperature electrical transport behaviors in textured $Ca_3Co_4O_9$-based polycrystalline ceramics, Appl. Phys. Lett. 94 (2009) 072107. https://doi.org/10.1063/1.3086875.

Figure Captions

Fig. 1. XRD patterns of the powdered $Ca_{3-x}Bi_xCo_4O_{9+\delta}$ samples at room temperature (Cu–K_α radiation): x = 0.0 (*1*), 0.2 (*2*), 0.3 (*3*), 0.5 (*4*), and 0.6 (*5*). The panel to the right shows an enlarged XRD patterns view at 2θ 15–20 degrees

Fig. 2. SEM images of the surface sections for sintered $Ca_{3-x}Bi_xCo_4O_{9+\delta}$ ceramic samples: (*a*) x = 0.0, (*b*) x = 0.2 (2), (*c*) x = 0.3, (*d*) x = 0.5, and (*e*) x = 0.6

Fig. 3. Element mapping images of the $Ca_3Co_4O_{9+\delta}$ (*a*) and $Ca_{2.8}Bi_{0.2}Co_4O_{9+\delta}$ (*b*) ceramic samples

Fig. 4. Temperature (*a*, *b*) and concentration (*c*, *d*) dependences of electrical resistivity (ρ) (*a*, *c*) and Seebeck coefficient (*S*) (*b*, *d*) of the $Ca_{3-x}Bi_xCo_4O_{9+\delta}$ ceramics: x = 0.0 (*1*), 0.2 (*2*), 0.3 (*3*), 0.5 (*4*), and 0.6 (*5*). I – single-phase samples, II – non-single-phase samples

Fig. 5. Temperature (*a*) and concentration (*b*) dependences of weighted mobility of charge carriers (μ) and their concentration (*p*) in the $Ca_{3-x}Bi_xCo_4O_{9+\delta}$ compounds: x = 0.0 (*1*), 0.2 (*2*), 0.3 (*3*), 0.5 (*4*), and 0.6 (*5*). I – homogeneous ceramics, II – heterogeneous ceramics

Fig. 6. Dependences of ln(σ*T*) versus reciprocal temperature for $Ca_{3-x}Bi_xCo_4O_{9+\delta}$ materials: x = 0.0 (*1*), 0.2 (*2*), 0.3 (*3*), 0.5 (*4*), and 0.6 (*5*). Inset shows concentration dependences of apparent activation of electrical conductivity of the samples below (6) and above (7) 573 K. I – homogeneous samples, II – heterogeneous samples

Fig. 7. Temperature (*a*, *b*) and concentration (*c*, *d*) dependences of thermal diffusivity (η) (*a*, *c*) and thermal conductivity (λ) (*b*, *d*) of the $Ca_{3-x}Bi_xCo_4O_{9+\delta}$ sintered ceramics: $x = 0.0$ (*1*), 0.2 (*2*), 0.3 (*3*), 0.5 (*4*), and 0.6 (*5*). I – single-phase region, II – non-single-phase region

Fig. 8. Temperature (*a*, *b*) and concentration (*c*, *d*) dependences of electron (λ_{el}) (*a*, *c*) and phonon (λ_{ph}) parts (*b*, *d*) of thermal conductivity of$Ca_{3-x}Bi_xCo_4O_{9+\delta}$ samples: $x = 0.0$ (*1*), 0.2 (*2*), 0.3 (*3*), 0.5 (*4*), and 0.6 (*5*). I – single-phase samples, II – non-single-phase samples

Fig. 9. Temperature (*a*, *b*) and concentration (*c*, *d*) dependences of power factor (*P*) (*a*, *c*) and figure-of-merit (*ZT*) (*b*, *d*) of $Ca_{3-x}Bi_xCo_4O_{9+\delta}$ oxide thermoelectrics: $x = 0.0$ (*1*), 0.2 (*2*), 0.3 (*3*), 0.5 (*4*), and 0.6 (*5*). I – homogeneous ceramics, II – composite ceramics

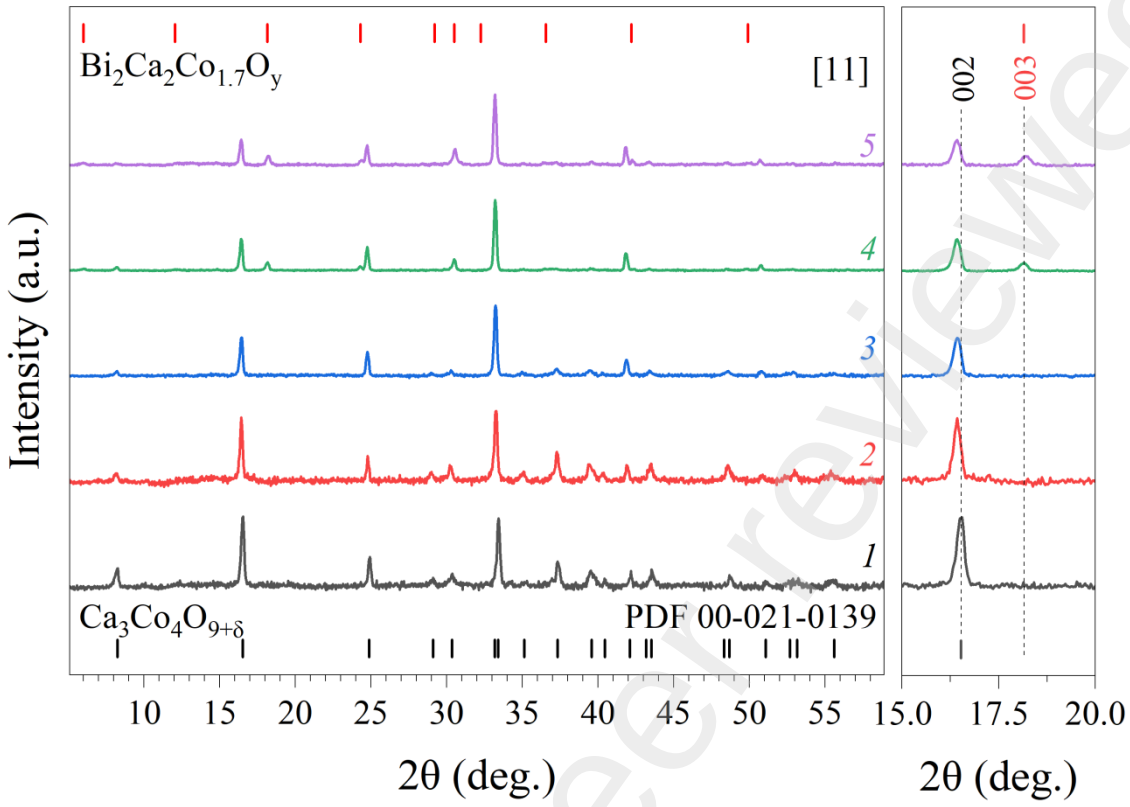

Fig. 1. XRD patterns of the powdered $Ca_{3-x}Bi_xCo_4O_{9+\delta}$ samples at room temperature (Cu–K_α radiation): x = 0.0 (*1*), 0.2 (*2*), 0.3 (*3*), 0.5 (*4*), and 0.6 (*5*). The panel to the right shows an enlarged XRD patterns view at 2θ 15–20 degrees

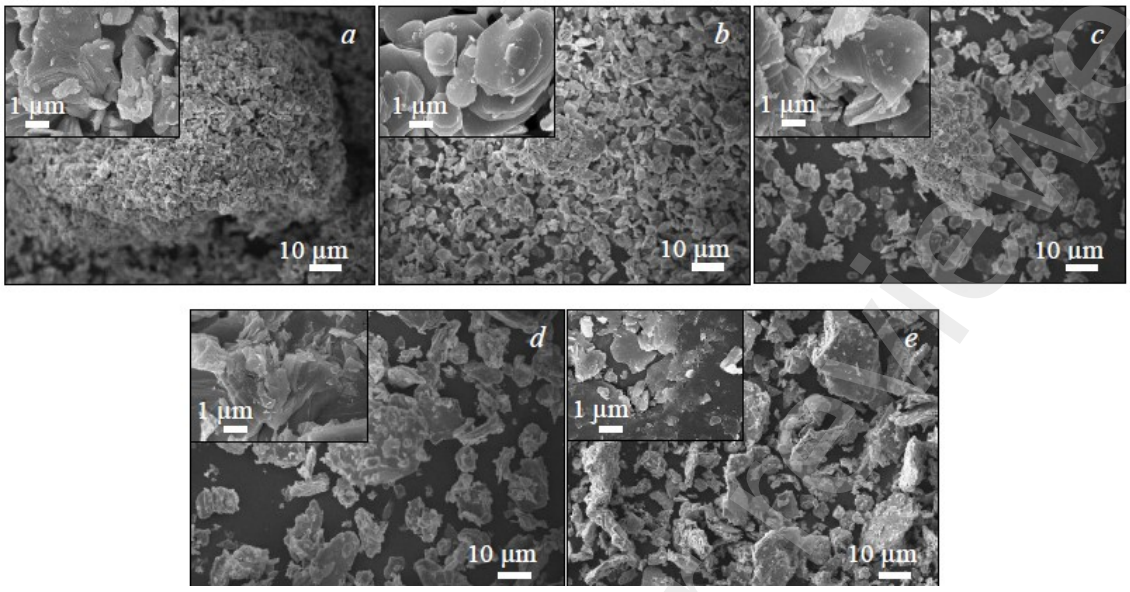

Fig. 2. SEM images of the surface sections for sintered $Ca_{3-x}Bi_xCo_4O_{9+\delta}$ ceramic samples: (*a*) $x = 0.0$, (*b*) $x = 0.2$ (2), (*c*) $x = 0.3$, (*d*) $x = 0.5$, and (*e*) $x = 0.6$

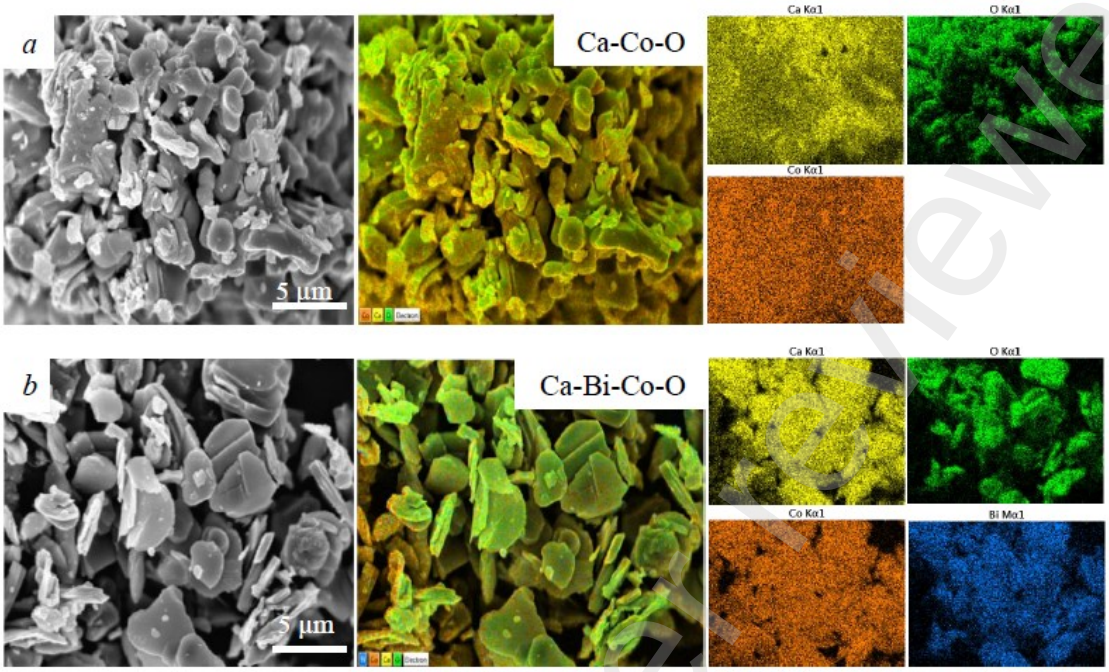

Fig. 3. Element mapping images of the $Ca_3Co_4O_{9+\delta}$ (*a*) and $Ca_{2.8}Bi_{0.2}Co_4O_{9+\delta}$ (*b*) ceramic samples

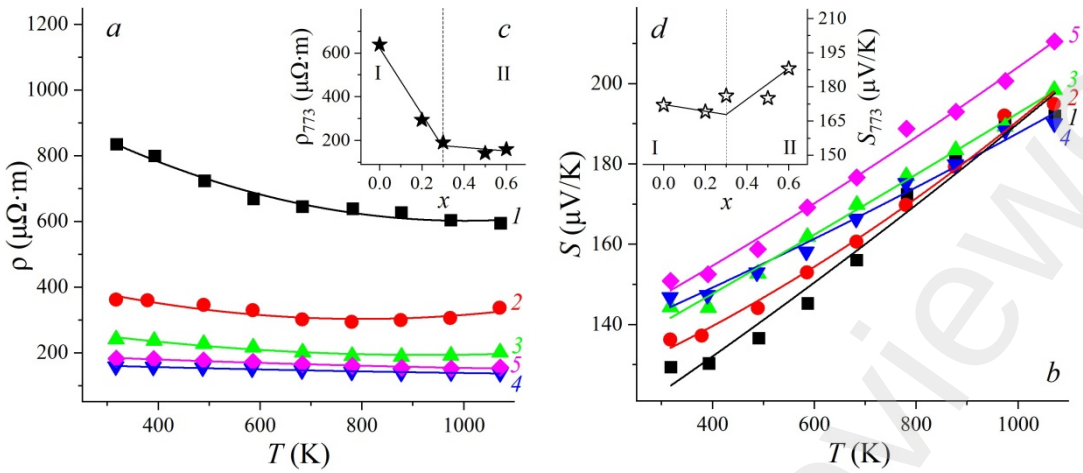

Fig. 4. Temperature (*a*, *b*) and concentration (*c*, *d*) dependences of electrical resistivity (ρ) (*a*, *c*) and Seebeck coefficient (*S*) (*b*, *d*) of the $Ca_{3-x}Bi_xCo_4O_{9+\delta}$ ceramics: x = 0.0 (*1*), 0.2 (*2*), 0.3 (*3*), 0.5 (*4*), and 0.6 (*5*). I – single-phase samples, II – non-single-phase samples

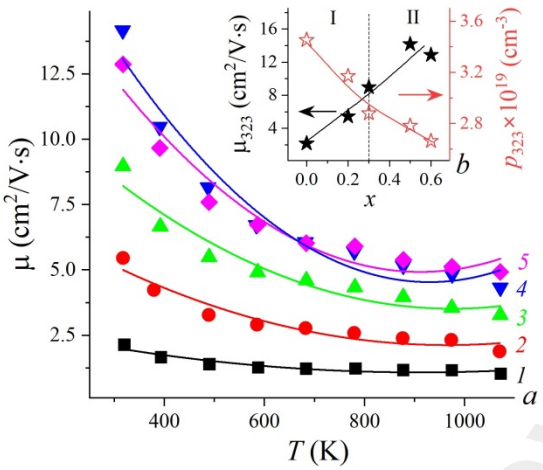

Fig. 5. Temperature (*a*) and concentration (*b*) dependences of weighted mobility of charge carriers (μ) and their concentration (*p*) in the $Ca_{3-x}Bi_xCo_4O_{9+\delta}$ compounds: x = 0.0 (*1*), 0.2 (*2*), 0.3 (*3*), 0.5 (*4*), and 0.6 (*5*). I – homogeneous ceramics, II – heterogeneous ceramics

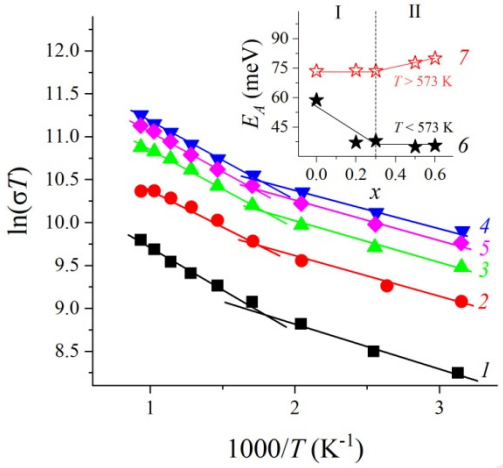

Fig. 6. Dependences of ln(σ*T*) versus reciprocal temperature for $Ca_{3-x}Bi_xCo_4O_{9+\delta}$ materials: x = 0.0 (*1*), 0.2 (*2*), 0.3 (*3*), 0.5 (*4*), and 0.6 (*5*). Inset shows concentration dependences of apparent activation of electrical conductivity of the samples below (6) and above (7) 573 K. I – homogeneous samples, II – heterogeneous samples

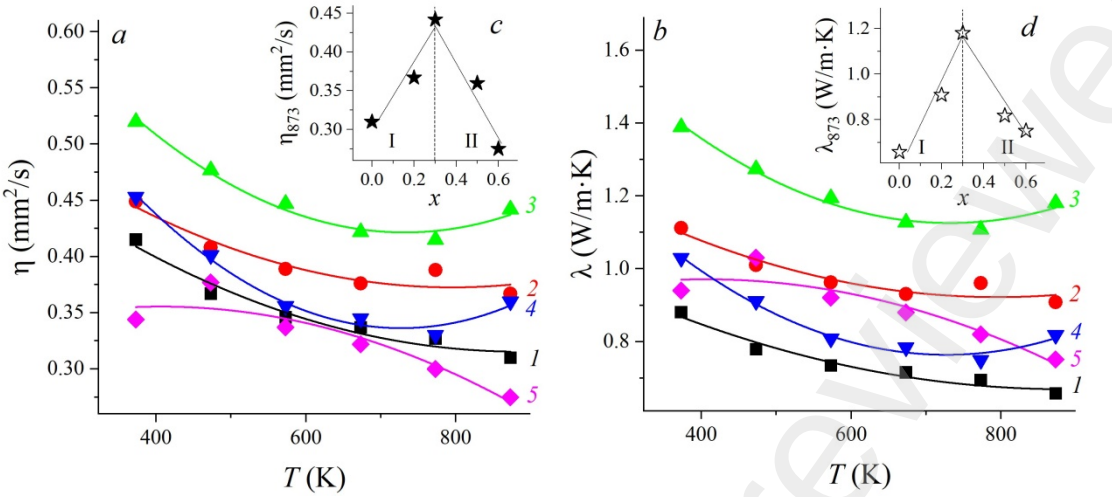

Fig. 7. Temperature (*a*, *b*) and concentration (*c*, *d*) dependences of thermal diffusivity (η) (*a*, *c*) and thermal conductivity (λ) (*b*, *d*) of the $Ca_{3-x}Bi_xCo_4O_{9+\delta}$ sintered ceramics: x = 0.0 (*1*), 0.2 (*2*), 0.3 (*3*), 0.5 (*4*), and 0.6 (*5*). I – single-phase region, II – non-single-phase region

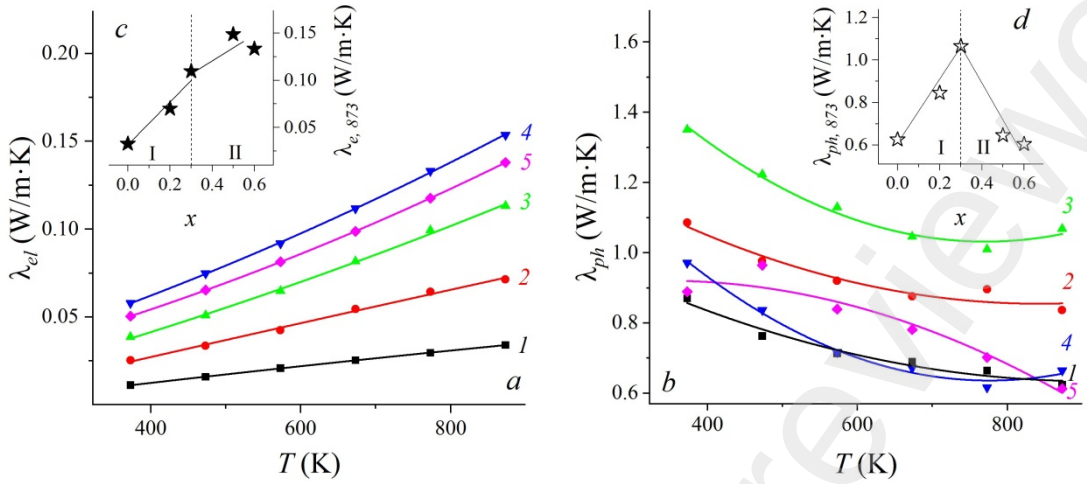

Fig. 8. Temperature (*a*, *b*) and concentration (*c*, *d*) dependences of electron (λ_{el}) (*a*, *c*) and phonon (λ_{ph}) parts (*b*, *d*) of thermal conductivity of $Ca_{3-x}Bi_xCo_4O_{9+\delta}$ samples: x = 0.0 (*1*), 0.2 (*2*), 0.3 (*3*), 0.5 (*4*), and 0.6 (*5*). I – single-phase samples, II – non-single-phase samples

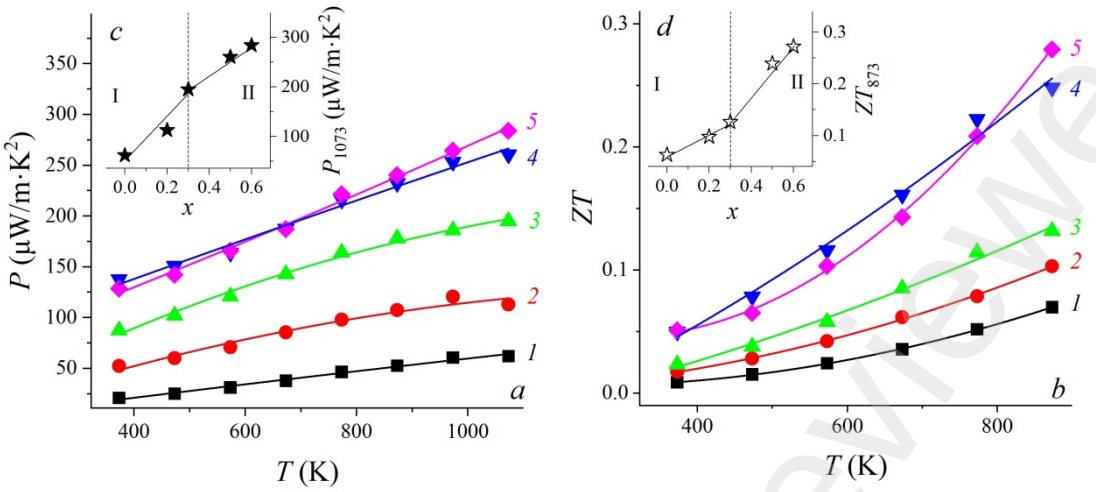

Fig. 9. Temperature (*a*, *b*) and concentration (*c*, *d*) dependences of power factor (*P*) (*a*, *c*) and figure-of-merit (*ZT*) (*b*, *d*) of $Ca_{3-x}Bi_xCo_4O_{9+\delta}$ oxide thermoelectrics: x = 0.0 (*1*), 0.2 (*2*), 0.3 (*3*), 0.5 (*4*), and 0.6 (*5*). I – homogeneous ceramics, II – composite ceramics

Tables Captions

Table 1. Values of pycnometric density of $Ca_{3-x}Bi_xCo_4O_{9+\delta}$ powders (d_{pow}) and ceramics (d_{cer}), and its porosity (Π)

Table 2. Nominal and real (obtained by EDX results) composition of the samples

Table 3. LTEC (α) values of $Ca_{3-x}Bi_xCo_4O_{9+\delta}$ ceramics

Table 4. Literature-reported functional characteristics of $Ca_3Co_4O_{9+\delta}$-based ceramics comparing with the results reported in this study

Table 1. Values of pycnometric density of $Ca_{3-x}Bi_xCo_4O_{9+\delta}$ powders (d_{pow}) and ceramics (d_{cer}), and its porosity (Π)

x	d_{pow} (g·cm^{-3})	d_{cer} (g·cm^{-3})	Π (%)
0.0	4.64	2.64	43.1
0.2	4.67	3.28	29.8
0.3	4.85	3.64	24.9
0.5	5.06	3.27	35.4
0.6	5.19	4.04	22.2

Table 2. Nominal and real (obtained by EDX results) composition of the samples

Sample	Nominal composition (mol. %)			Real composition (mol. %)		
	$BiO_{1.5}$	CaO	CoO_x	$BiO_{1.5}$	CaO	CoO_x
$Ca_3Co_4O_{9+\delta}$	–	42.86	57.14	–	39.76	60.24
$Ca_{2.8}Bi_{0.2}Co_4O_{9+\delta}$	2.86	40.00	57.14	2.96	33.88	63.16
$Ca_{2.7}Bi_{0.3}Co_4O_{9+\delta}$	4.29	38.57	57.14	4.71	32.86	62.43
$Ca_{2.5}Bi_{0.5}Co_4O_{9+\delta}$	7.14	35.71	57.14	7.78	30.40	61.83
$Ca_{2.4}Bi_{0.6}Co_4O_{9+\delta}$	8.57	34.29	57.14	12.31	30.00	57.69

Table 3. LTEC (α) values of $Ca_{3-x}Bi_xCo_4O_{9+\delta}$ ceramics

x	0.0	0.2	0.3	0.5	0.6
$\alpha \cdot 10^6$, K^{-1}	13.17±0.66	13.00±0.65	12.80±0.64	11.60±0.58	12.48±0.62

Table 4. Literature-reported functional characteristics of $Ca_3Co_4O_{9+\delta}$-based ceramics comparing with the results reported in this study

Formula	Synthesis method	Sintering method	Measurement temperature, K	ρ, μΩ·m	*S*, μV/K	*P*, μW/m·K²	λ, W/m·K	*ZT*	Year	Ref
$Ca_{2.5}Bi_{0.5}Co_4O_{9+\delta}$	SSR	CS	973	95	160	270	1.34	0.2	2000	[17]
$Ca_{2.85}Bi_{0.15}Co_4O_{9+\delta}$	Sol-gel	SPS	973	69	179	461	1.81	0.25	2008	[45]
$Ca_{2.9}Bi_{0.1}Co_4O_{9+\delta}$ (air) $Ca_{2.85}Bi_{0.15}Co_4O_{9+\delta}$ (air) $Ca_{2.8}Bi_{0.2}Co_4O_{9+\delta}$ (Ar) $Ca_{2.8}Bi_{0.2}Co_4O_{9+\delta}$ (air)	SSR	HP + post annealing at 973 K (on air or Ar)	870 870 870 870	87 98 189 118	160 171 197 170	294 298 206 246	- - 1.16 -	0.16 0.18 0.15 0.19	2011	[48]
$Ca_{2.7}Bi_{0.3}Co_{3.9}Fe_{0.1}O_{9+\delta}$	SSR	SPS	973	74	182	451	1.18	0.4	2014	[18]
$Ca_3Co_4O_{9+\delta}$ / 10 wt % Ag	Sol-gel	TSS	1073	100	210	430	-	-	2015	[33]
$Ca_{2.9}Cd_{0.1}Co_4O_{9+\delta}$ / 10 wt % Ag	SSR	HP	952	41	189	880	2.72	0.31	2019	[9]
$Ca_3Co_4O_{9+\delta}$ / 2 wt % Cu	GCN process	HP	1100	87	211	521	-	0.223	2020	[34]
$Ca_3Co_4O_{9+\delta}$ / 0.05 wt % SiC	SSR	CS	923	105	195	365	1.54	0.218	2020	[37]
$Ca_{2.7}Bi_{0.3}Co_{3.92}O_{9+\delta}$	SSR	SPS + post annealing at 1023 K	823	80	160	340	1.79	0.16	2020	[57]
$Ca_3Co_4O_{9+\delta}$ / 0.75 wt % TiC $Ca_3Co_4O_{9+\delta}$ / 0.25 wt % TiC	SSR	CS	1073 1073	145 170	195 194	262 222	1.82 1.47	0.15 0.16	2021	[38]
$Ca_{2.4}Bi_{0.6}Co_4O_{9+\delta}$	SSR	CS	1073 873	156	211	284 240	0.75	0.28	2025	This work

SSR – solid state reaction; GCN process – glycine-citrate-nitrate process; CS – conventional sintering; SPS – spark-plasma sintering; HP – hot pressing; TSS – two-step sintering

Figure Captions

Fig. 1. XRD patterns of the powdered $Ca_{3-x}Bi_xCo_4O_{9+\delta}$ samples at room temperature (Cu–K_α radiation): x = 0.0 (*1*), 0.2 (*2*), 0.3 (*3*), 0.5 (*4*), and 0.6 (*5*). The panel to the right shows an enlarged XRD patterns view at 2θ 15–20 degrees

Fig. 2. SEM images of the surface sections for sintered $Ca_{3-x}Bi_xCo_4O_{9+\delta}$ ceramic samples: (*a*) x = 0.0, (*b*) x = 0.2 (2), (*c*) x = 0.3, (*d*) x = 0.5, and (*e*) x = 0.6

Fig. 3. Element mapping images of the $Ca_3Co_4O_{9+\delta}$ (*a*) and $Ca_{2.8}Bi_{0.2}Co_4O_{9+\delta}$ (*b*) ceramic samples

Fig. 4. Temperature (*a*, *b*) and concentration (*c*, *d*) dependences of electrical resistivity (ρ) (*a*, *c*) and Seebeck coefficient (*S*) (*b*, *d*) of the $Ca_{3-x}Bi_xCo_4O_{9+\delta}$ ceramics: x = 0.0 (*1*), 0.2 (*2*), 0.3 (*3*), 0.5 (*4*), and 0.6 (*5*). I – single-phase samples, II – non-single-phase samples

Fig. 5. Temperature (*a*) and concentration (*b*) dependences of weighted mobility of charge carriers (μ) and their concentration (*p*) in the $Ca_{3-x}Bi_xCo_4O_{9+\delta}$ compounds: x = 0.0 (*1*), 0.2 (*2*), 0.3 (*3*), 0.5 (*4*), and 0.6 (*5*). I – homogeneous ceramics, II – heterogeneous ceramics

Fig. 6. Dependences of $\ln(\sigma T)$ versus reciprocal temperature for $Ca_{3-x}Bi_xCo_4O_{9+\delta}$ materials: x = 0.0 (*1*), 0.2 (*2*), 0.3 (*3*), 0.5 (*4*), and 0.6 (*5*). Inset shows concentration dependences of apparent activation of electrical conductivity of the samples below (6) and above (7) 573 K. I – homogeneous samples, II – heterogeneous samples

Fig. 7. Temperature (*a*, *b*) and concentration (*c*, *d*) dependences of thermal diffusivity (η) (*a*, *c*) and thermal conductivity (λ) (*b*, *d*) of the $Ca_{3-x}Bi_xCo_4O_{9+\delta}$ sintered ceramics: x = 0.0 (*1*), 0.2 (*2*), 0.3 (*3*), 0.5 (*4*), and 0.6 (*5*). I – single-phase region, II – non-single-phase region

Fig. 8. Temperature (*a*, *b*) and concentration (*c*, *d*) dependences of electron (λ_{el}) (*a*, *c*) and phonon (λ_{ph}) parts (*b*, *d*) of thermal conductivity of$Ca_{3-x}Bi_xCo_4O_{9+\delta}$ samples: x = 0.0 (*1*),

0.2 (*2*), 0.3 (*3*), 0.5 (*4*), and 0.6 (*5*). I – single-phase samples, II – non-single-phase samples

Fig. 9. Temperature (*a*, *b*) and concentration (*c*, *d*) dependences of power factor (*P*) (*a*, *c*) and figure-of-merit (*ZT*) (*b*, *d*) of $Ca_{3-x}Bi_xCo_4O_{9+\delta}$ oxide thermoelectrics: $x = 0.0$ (*1*), 0.2 (*2*), 0.3 (*3*), 0.5 (*4*), and 0.6 (*5*). I – homogeneous ceramics, II – composite ceramics

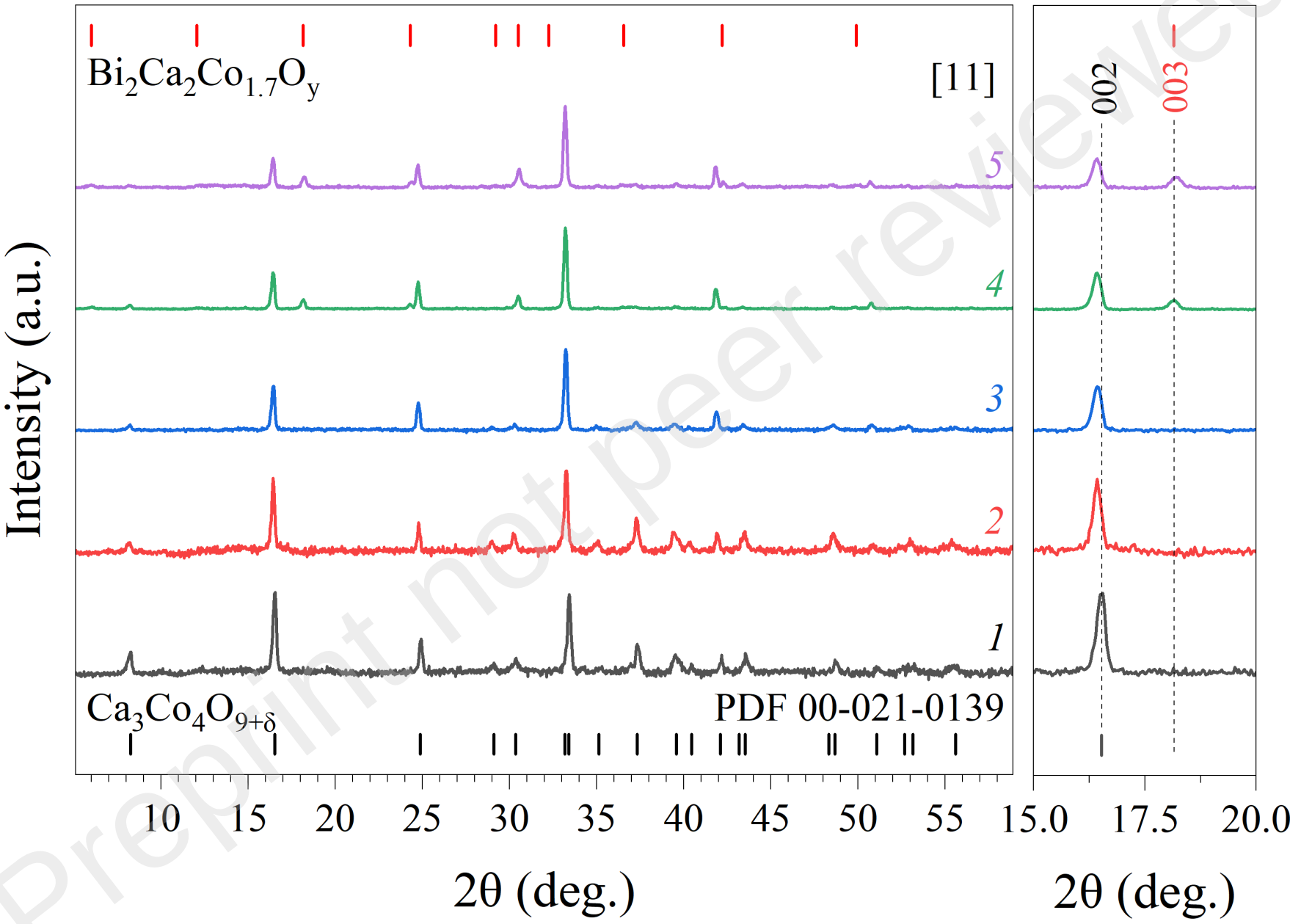

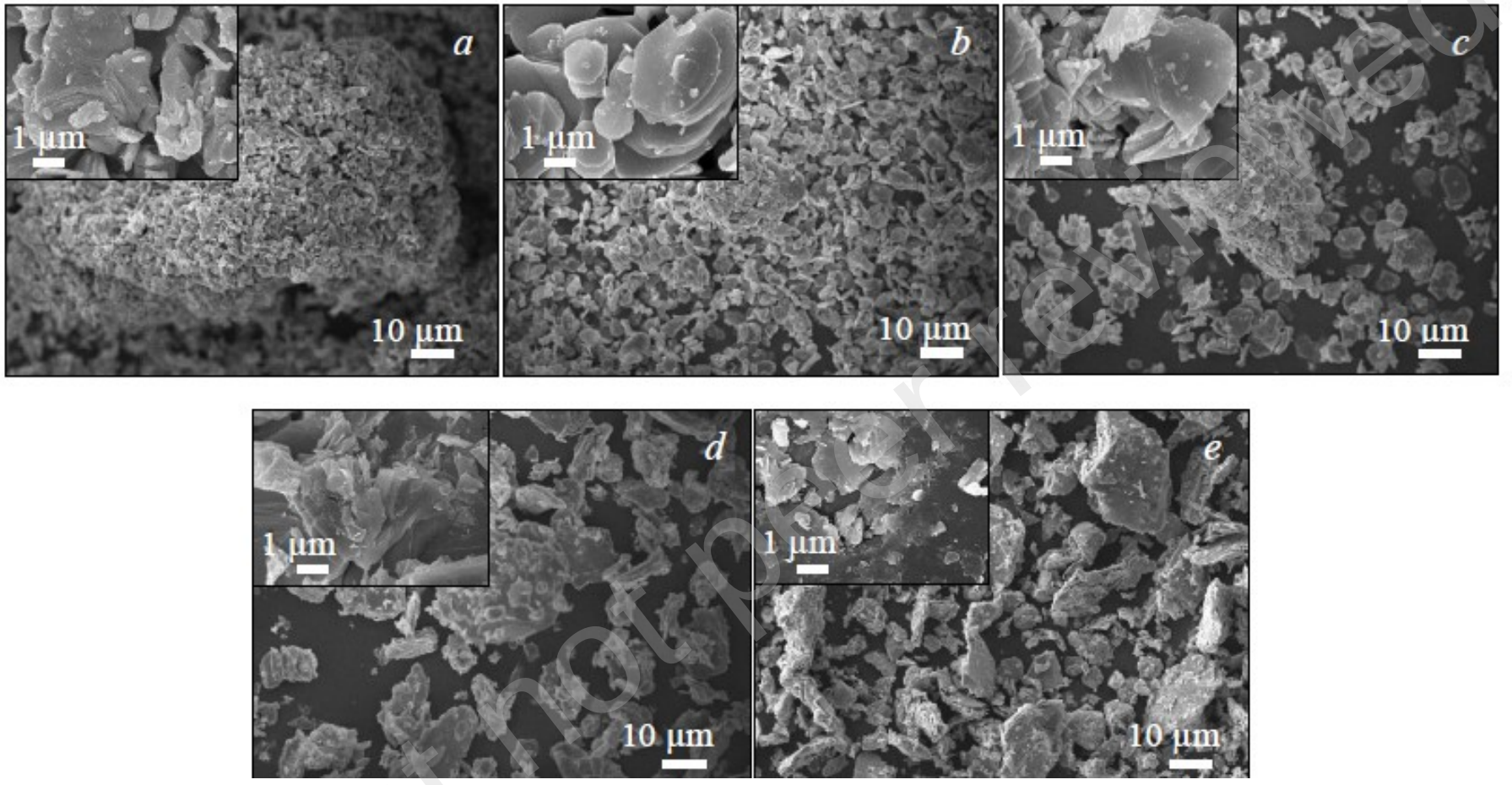

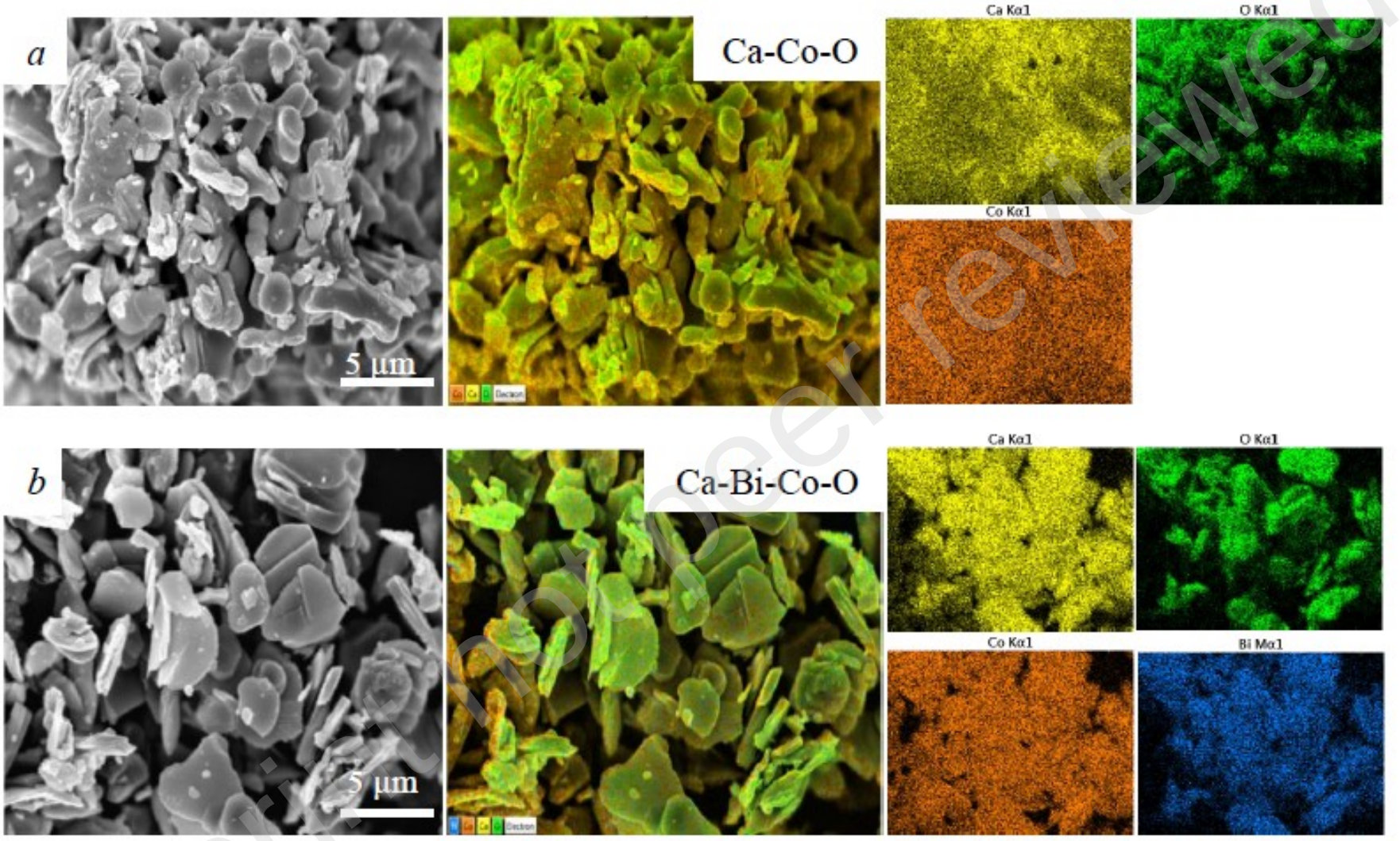

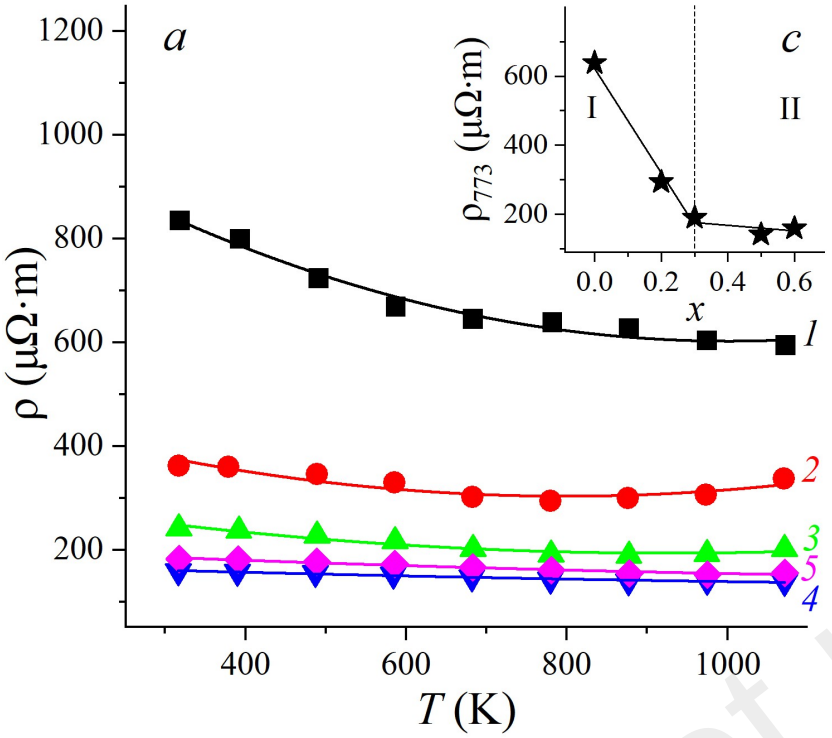

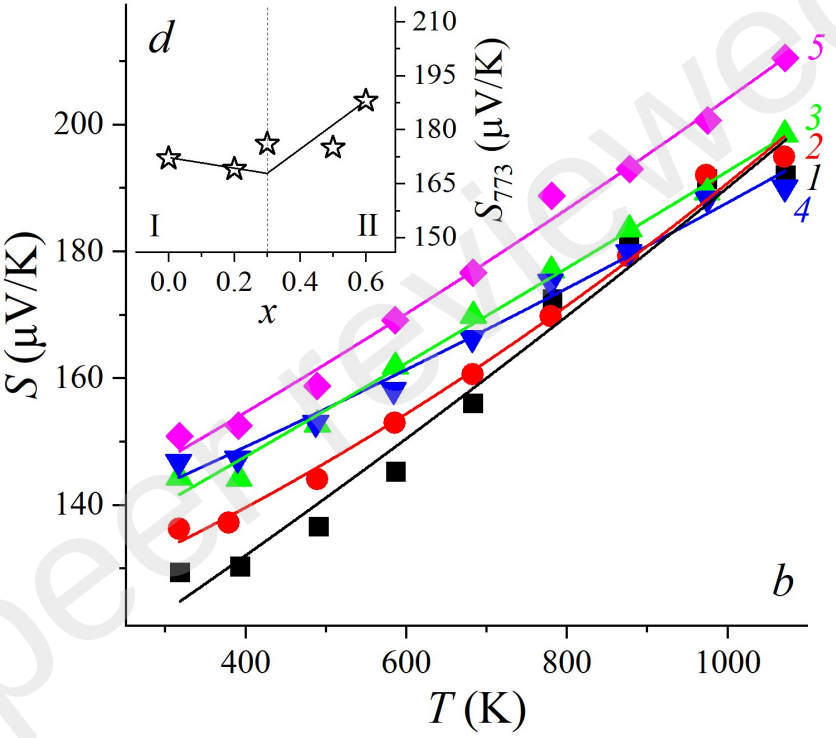

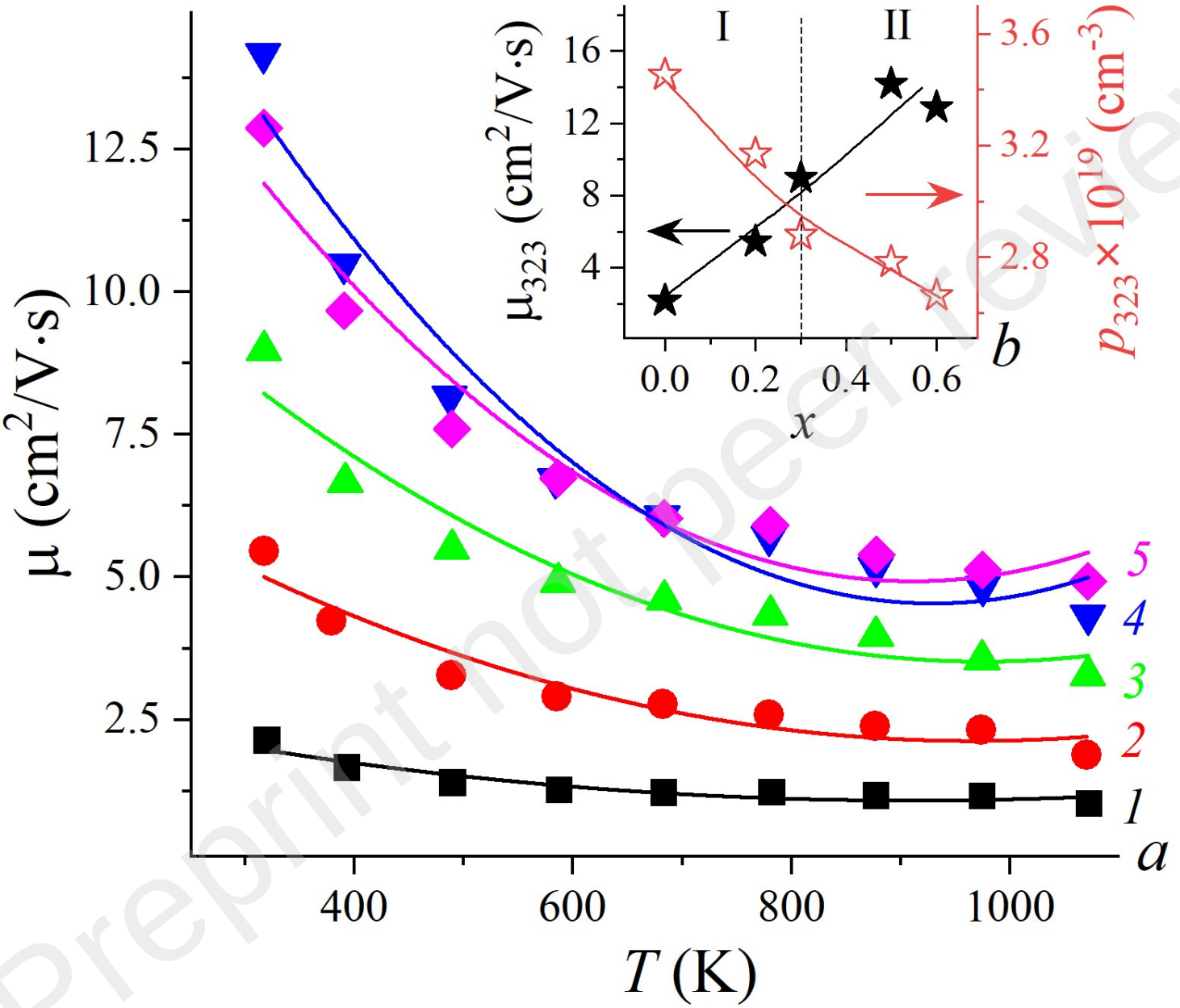

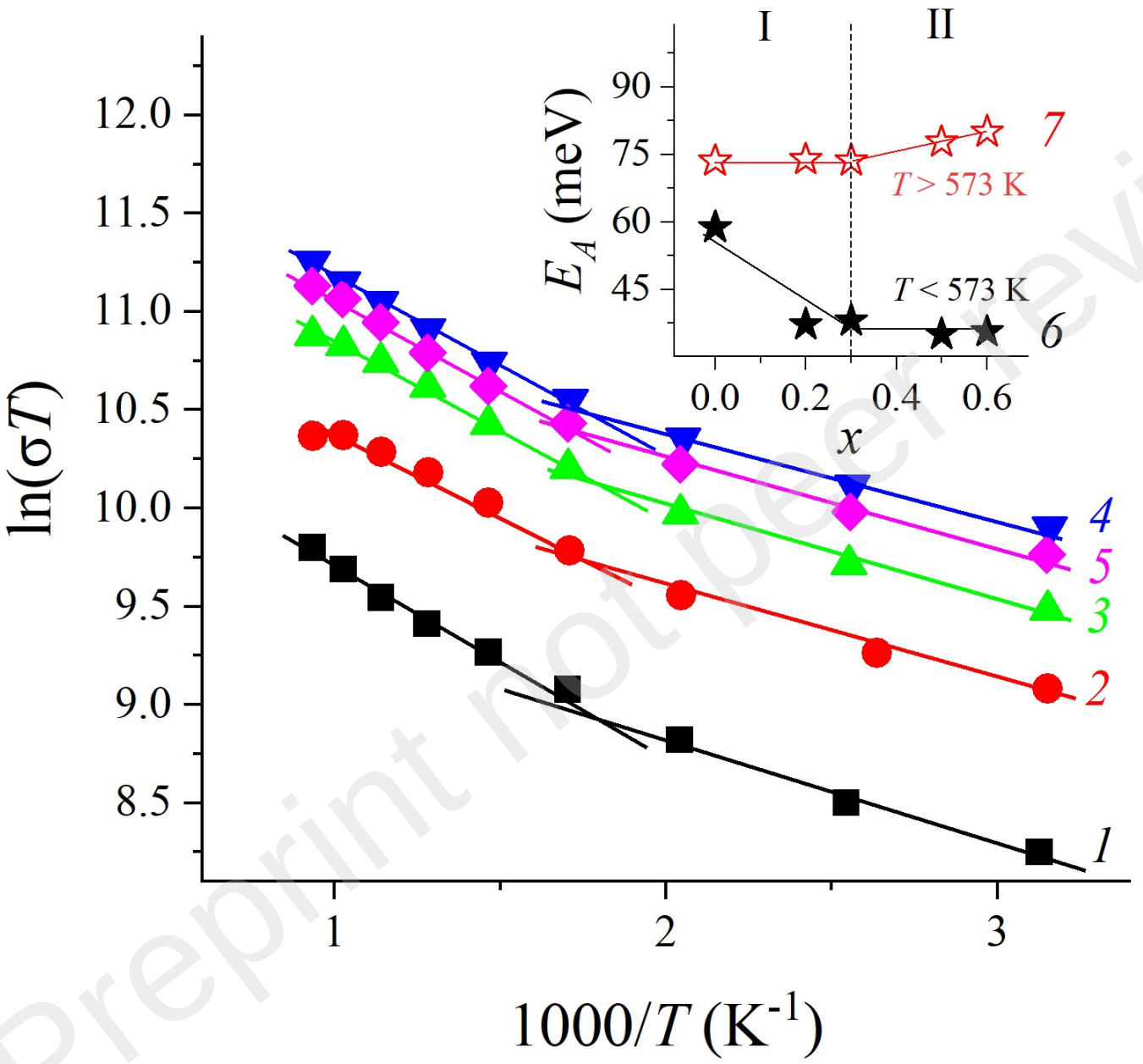

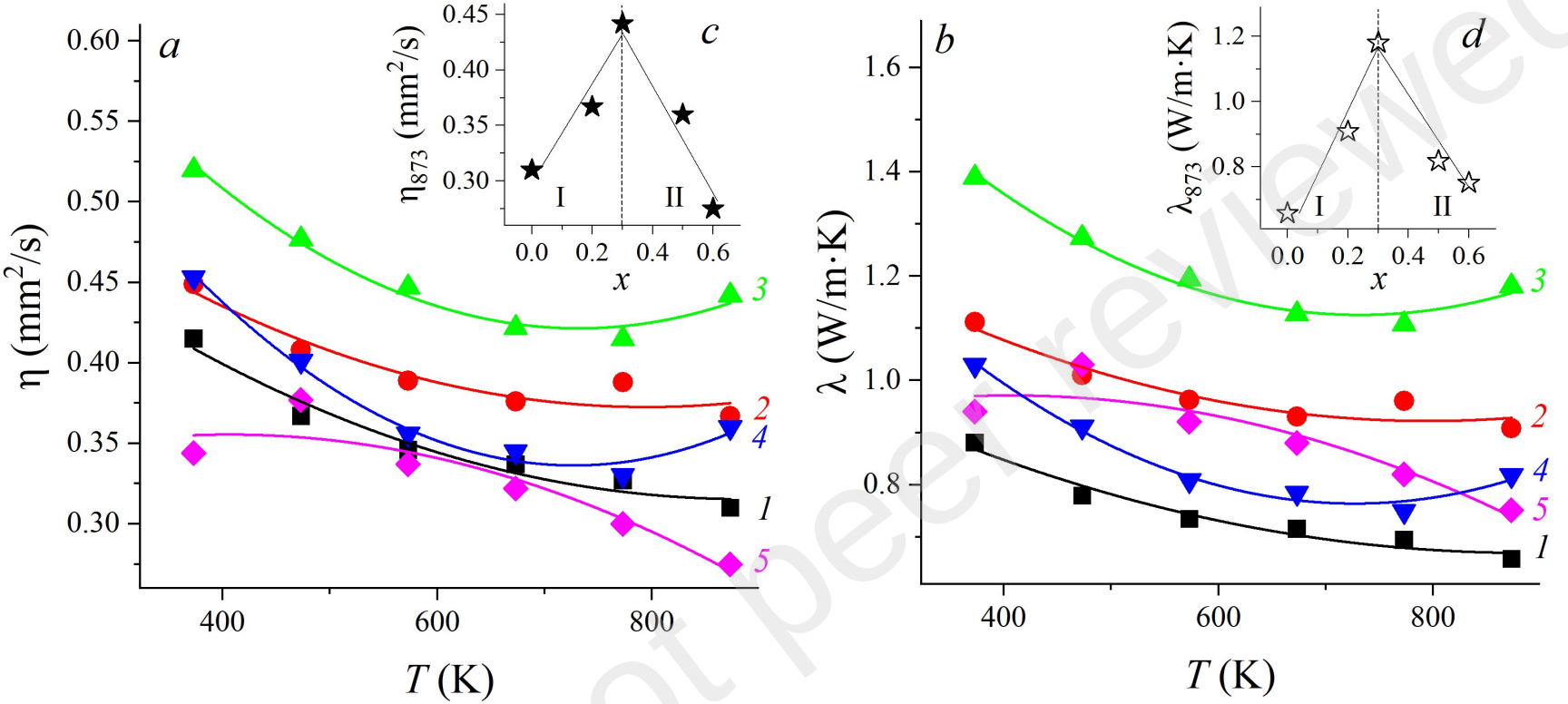

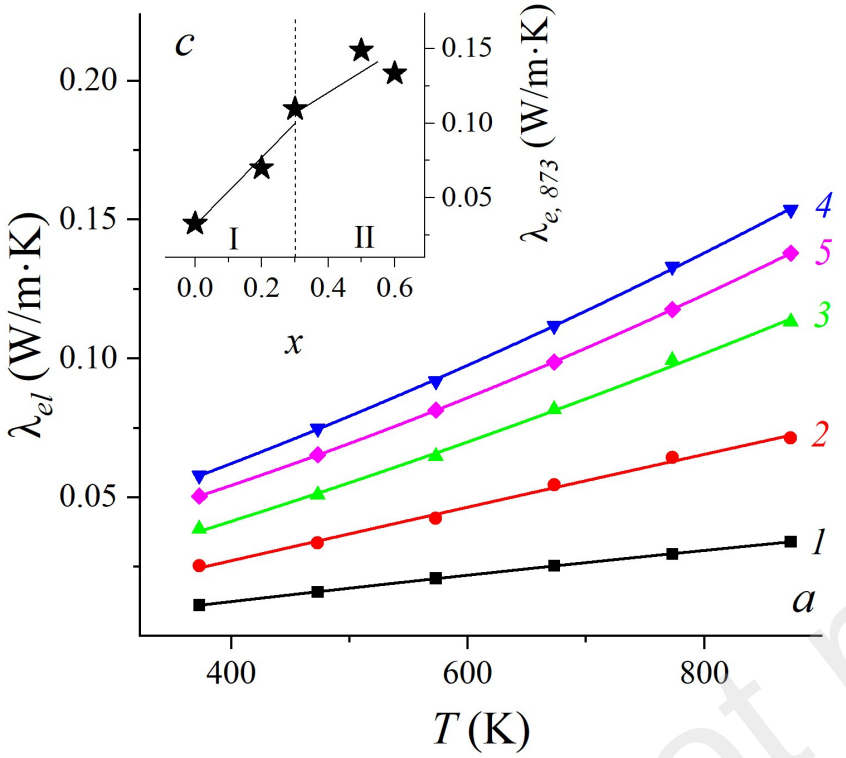

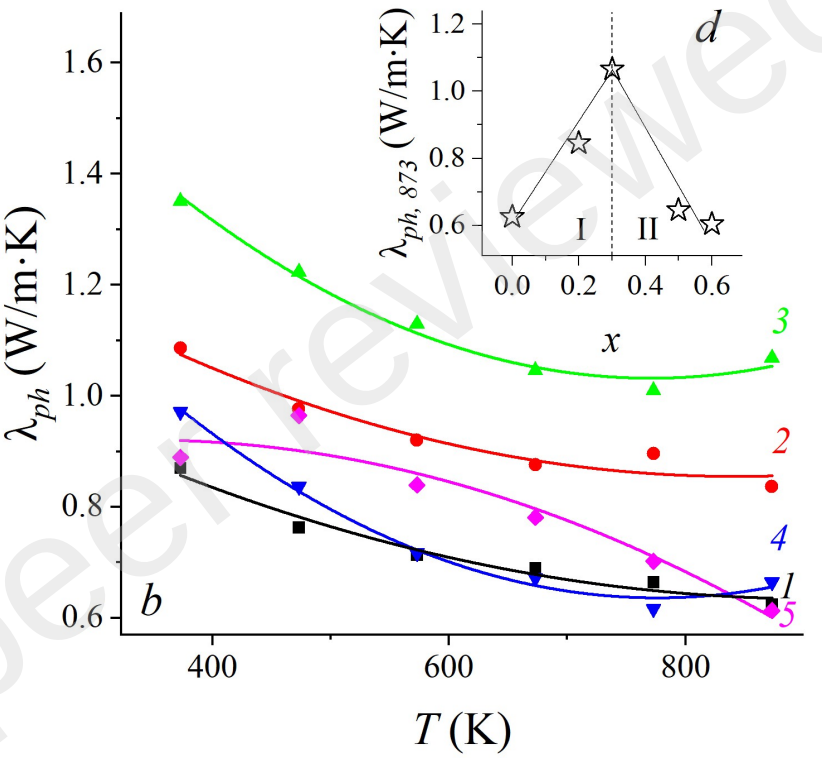

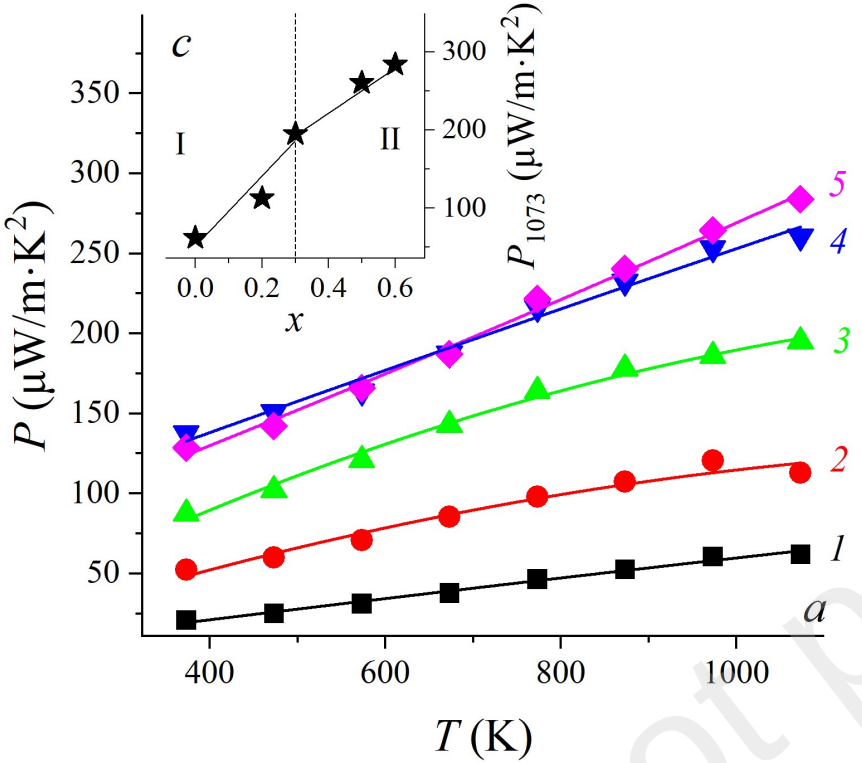

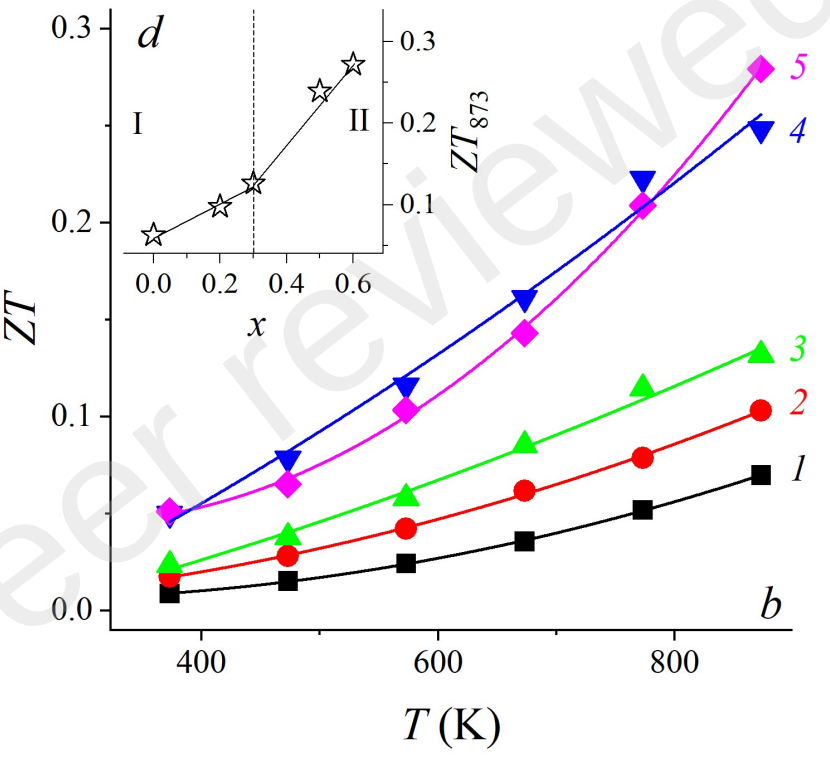

Tables Captions

Table 1. Values of pycnometric density of $Ca_{3-x}Bi_xCo_4O_{9+\delta}$ powders (d_{pow}) and ceramics (d_{cer}), and its porosity (Π)

Table 2. Nominal and real (obtained by EDX results) composition of the samples

Table 3. LTEC (α) values of $Ca_{3-x}Bi_xCo_4O_{9+\delta}$ ceramics

Table 4. Literature-reported functional characteristics of $Ca_3Co_4O_{9+\delta}$-based ceramics comparing with the results reported in this study

Table 1. Values of pycnometric density of $Ca_{3-x}Bi_xCo_4O_{9+\delta}$ powders (d_{pow}) and ceramics (d_{cer}), and its porosity (Π)

x	d_{pow}(g·cm^{-3})	d_{cer} (g·cm^{-3})	Π (%)
0.0	4.64	2.64	43.1
0.2	4.67	3.28	29.8
0.3	4.85	3.64	24.9
0.5	5.06	3.27	35.4
0.6	5.19	4.04	22.2

Table 2. Nominal and real (obtained by EDX results) composition of the samples

Sample	Nominal composition (mol. %)			Real composition (mol. %)		
	$BiO_{1.5}$	CaO	CoO_x	$BiO_{1.5}$	CaO	CoO_x
$Ca_3Co_4O_{9+\delta}$	–	42.86	57.14	–	39.76	60.24
$Ca_{2.8}Bi_{0.2}Co_4O_{9+\delta}$	2.86	40.00	57.14	2.96	33.88	63.16
$Ca_{2.7}Bi_{0.3}Co_4O_{9+\delta}$	4.29	38.57	57.14	4.71	32.86	62.43
$Ca_{2.5}Bi_{0.5}Co_4O_{9+\delta}$	7.14	35.71	57.14	7.78	30.40	61.83
$Ca_{2.4}Bi_{0.6}Co_4O_{9+\delta}$	8.57	34.29	57.14	12.31	30.00	57.69

Table 3. LTEC (α) values of $Ca_{3-x}Bi_xCo_4O_{9+\delta}$ ceramics

x	0.0	0.2	0.3	0.5	0.6
$\alpha \cdot 10^6$, K^{-1}	13.17±0.66	13.00±0.65	12.80±0.64	11.60±0.58	12.48±0.62

Table 4. Literature-reported functional characteristics of $Ca_3Co_4O_{9+\delta}$-based ceramics comparing with the results reported in this study

Formula	Synthesis method	Sintering method	Measurement temperature, K	ρ, μΩ·m	*S*, μV/K	*P*, μW/m·K²	λ, W/m·K	*ZT*	Year	Ref
$Ca_{2.5}Bi_{0.5}Co_4O_{9+\delta}$	SSR	CS	973	95	160	270	1.34	0.2	2000	[17]
$Ca_{2.85}Bi_{0.15}Co_4O_{9+\delta}$	Sol-gel	SPS	973	69	179	461	1.81	0.25	2008	[45]
$Ca_{2.9}Bi_{0.1}Co_4O_{9+\delta}$ (air) $Ca_{2.85}Bi_{0.15}Co_4O_{9+\delta}$ (air) $Ca_{2.8}Bi_{0.2}Co_4O_{9+\delta}$ (Ar) $Ca_{2.8}Bi_{0.2}Co_4O_{9+\delta}$ (air)	SSR	HP + post annealing at 973 K (on air or Ar)	870 870 870 870	87 98 189 118	160 171 197 170	294 298 206 246	- - 1.16 -	0.16 0.18 0.15 0.19	2011	[48]
$Ca_{2.7}Bi_{0.3}Co_{3.9}Fe_{0.1}O_{9+\delta}$	SSR	SPS	973	74	182	451	1.18	0.4	2014	[18]
$Ca_3Co_4O_{9+\delta}$ / 10 wt % Ag	Sol-gel	TSS	1073	100	210	430	-	-	2015	[33]
$Ca_{2.9}Cd_{0.1}Co_4O_{9+\delta}$ / 10 wt % Ag	SSR	HP	952	41	189	880	2.72	0.31	2019	[9]
$Ca_3Co_4O_{9+\delta}$ / 2 wt % Cu	GCN process	HP	1100	87	211	521	-	0.223	2020	[34]
$Ca_3Co_4O_{9+\delta}$ / 0.05 wt % SiC	SSR	CS	923	105	195	365	1.54	0.218	2020	[37]
$Ca_{2.7}Bi_{0.3}Co_{3.92}O_{9+\delta}$	SSR	SPS + post annealing at 1023 K	823	80	160	340	1.79	0.16	2020	[57]
$Ca_3Co_4O_{9+\delta}$ / 0.75 wt % TiC $Ca_3Co_4O_{9+\delta}$ / 0.25 wt % TiC	SSR	CS	1073 1073	145 170	195 194	262 222	1.82 1.47	0.15 0.16	2021	[38]
$Ca_{2.4}Bi_{0.6}Co_4O_{9+\delta}$	SSR	CS	1073 873	156	211	284 240	0.75	0.28	2025	This work

SSR – solid state reaction; GCN process – glycine-citrate-nitrate process; CS – conventional sintering; SPS – spark-plasma sintering; HP – hot pressing; TSS – two-step sintering